Energy 347 (2026) 140313

Contents lists available at ScienceDirect

Energy

journal homepage: www.elsevier.com/locate/energy

Techno-economic-environmental analysis of a PVT-based solar combined cooling, heating, and power system

Jeremias E. Castro [a], Andreas V. Olympios [b,c], Asmaa A. Harraz [d,*], Bryce S. Richards [a], Jingyuan Xu [a,*]

[a] Institute of Microstructure Technology, Karlsruhe Institute of Technology, Karlsruhe, 76344, Germany
[b] PHAETHON Centre of Excellence for Intelligent, Efficient and Sustainable Energy Solutions, Nicosia, Cyprus
[c] PV Technology Laboratory, Department of Electrical and Computer Engineering, University of Cyprus, Nicosia, Cyprus
[d] Environmental Engineering Program, University of Science and Technology, Zewail City of Science and Technology, Egypt

ARTICLE INFO

Keywords:
Photovoltaic-thermal (PVT) collectors
Diffusion absorption refrigeration (DAR)
Solar combined cooling, heating and power (S-CCHP)
Electricity-free cooling
Residential energy
Techno-economic analysis

ABSTRACT

The growing adoption of solar energy in the residential sector plays a pivotal role in advancing sustainable energy practices, reducing carbon dioxide emissions, and enhancing energy independence. This study examines a solar combined cooling, heating, and power (S-CCHP) system incorporating photovoltaicthermal (PVT) technology and assesses its performance alongside alternative photovoltaic (PV) and solar thermal (ST) configurations. A transient model is developed, together with economic and environmental assessments, to simulate overall energy performance, including the use of thermal energy from the PVT system to support summer cooling via a diffusion absorption refrigeration (DAR) cycle without using electricity during summer months. All system configurations are analysed under different layouts, both with and without battery storage. As a case study, the system is designed for application in Berlin, Germany, and the results show that the PVT-based system can supply 68% of domestic hot water demand and 48% of appliance electricity use, but only 12% of space heating due to the limited temperature output of the PVT collectors. Importantly, while the DAR system achieves full coverage of space cooling demand in summer, it relies heavily on auxiliary thermal energy input, underscoring a key area for system improvement. The economic analysis indicates net present values of approximately €7800 for PVT, €11,300 for ST, and €23,600 for PV, with corresponding payback periods of 21.0, 16.5, and 6.9 years. In terms of environmental performance, the PVT-based system achieves the highest carbon dioxide emission reduction at 2658 kg/year, followed by the PV (1904 kg/year) and ST (1781 kg/year) systems. The sensitivity analysis highlights the critical role of battery integration, especially under high grid electricity prices. In conclusion, the PVT-based S-CCHP system demonstrates strong economic and environmental potential in urban environments, while the DAR integration offers a compelling pathway for electricity-free cooling, revealing significant opportunities for optimisation and future development.

1. Introduction

The urgency to combat climate change and transition to sustainable energy sources is increasingly apparent [1], with the energy sector playing a central role in reducing carbon dioxide (CO_2) and other greenhouse gas emissions [2,3]. As of 2024, global CO_2 emissions from this sector reached approximately 37.8 $GtCO_2$, with the buildings segment contributing around 10 $GtCO_2$ in 2022 alone [4,5]. Renewable energy sources, notably solar and wind, are crucial to this transition [6], yet their intermittent nature presents challenges for integration into existing energy systems [7]. Policies targeting net-zero energy and emissions in buildings, such as those in the European Union, drive the adoption of solar technologies, which in urban contexts offer energy independence, resilience, and environmental benefits despite persistent hurdles in fully harnessing their potential [8–11]. Amidst these challenges, the integration of advanced renewable energy technologies, such as photovoltaic-thermal (PVT) systems, offers opportunities to optimise solar energy use and mitigate emissions within the buildings sector, particularly when rooftop availability is limited, as PVT systems simultaneously generate electricity and heat using the same aperture area [12,13]. By maximising energy use per square meter and reducing PV cell operating temperatures, PVT systems improve overall system efficiency and reduce the environmental footprint of buildings [12,14,15]. Multiple PVT configurations exist,

* Corresponding authors.
E-mail addresses: aharraz@zewailcity.edu.eg (A.A. Harraz), jingyuan.xu@kit.edu (J. Xu).

https://doi.org/10.1016/j.energy.2026.140313
Received 27 October 2025; Received in revised form 27 January 2026; Accepted 2 February 2026
Available online 3 February 2026

Nomenclature

Acronyms

COP	Coefficient of performance
DAR	Diffusion absorption refrigeration
EMAT	Exchanger minimum approach temperature
HW	Hot water
MPP	Maximum power point
NPV	Net present value
PBT	Payback time
PV	Photovoltaic
PVT	Photovoltaic-thermal
S-CCHP	Solar combined cooling, heating, and power
SC	Space cooling
SH	Space heating
ST	Solar thermal

Variables

A	Area, m^2
a_1, a_2	Heat loss coefficients, $W/(m^2\ K)$ and $W/(m^2\ K^2)$
AAD	Average absolute deviation
C	Cost, €
c	Purchase cost, €/kWh
c_p	Specific heat capacity, J/(kg K)
D	Diameter, m
d	Discount rate
E	Electrical energy, kWh
$\dot{E}$	Electrical power, W
e, p, g, j	Fitting constants in Eq. (8)
f	Emission factors, or Darcy–Weisbach friction factor
G	Solar irradiance, W/m^2
h	Heat transfer coefficient, $W/(m^2\ K)$
i_f	Inflation rate
I_o	Initial investment, €
k	Thermal conductivity, W/(m K)
L	Pipe length, m
m	Mass in kg, or empirical constant in equation A.5
$\dot{m}$	Mass flow rate, kg/s
N	Number of modules/units or points
n	Investment horizon, years
P	Pressure, Pa
Q	Thermal energy, kWh
$\dot{Q}$	Thermal power, W
q''	Heat flux, W/m^2
R	Thermal resistance, K/W
s	Selling price, €/kWh
T	Temperature, °C or K
U	Overall heat transfer coefficient, $W/(m^2\ K)$
v, x, y, z	Fitting constants in Eq. (9)
$\dot{W}$	Pump power, W
X_i	Experimental and calculated values

Greek symbols

β	Power temperature coefficient
ε	Effectiveness
η	Efficiency
μ	Dynamic viscosity, Pa s
ρ	Density, kg/m^3

Subscripts and Superscripts

abs	Absorber
amb	Ambient
calc	Calculated
c	Collector
coil	Coil heat exchanger
cov	Covered
dem	Demand
elec	Electric
eqel	Equivalent electricity
exc	Excess electricity
exp	Experimental
fa	Fluid through heat exchanger coil
fu	Fluid through each PVT collector
gen	Generator
hw	Hot water
i	Inside
loss	Losses
mod	Module
MPP	Maximum power point
ng	Natural gas
o	Outside
p	Pipe
rec	Rectifier
r	Reduced
sc	Space cooling
sh	Space heating
th	Thermal
wt	Water tank

Units

€/c	Euros per collector
€/kWh	Euros per kilowatt-hour
€/kWp	Euros per kilowatt peak
€/L	Euros per litre
€/m^2	Euros per square meter
$GtCO_2$	Gigatonnes of carbon dioxide
$kgCO_2/kWh$	Kilograms of CO_2 emitted per kilowatt-hour
L/hůc	Litres per hour per collector

including air-based, liquid-based, heat-pipe, dual air/water, and concentrating systems [16–19], each suited to different climates, space constraints, and energy demand profiles [12]. Among them, water-based PVT systems stand out due to their high technology readiness (TRL 9) and commercial availability [12,20], using water as the heat transfer fluid and performing effectively in year-round water preheating applications [12]. The choice between uncovered and covered designs further affects thermal performance [20], with covered PVT systems offering higher thermal efficiency and being recommended when heat production is prioritised over electricity generation [20].

As a complementary technology to PVT systems, thermally-driven refrigeration provides a solution for meeting cooling demands in buildings without relying on conventional mechanical compression systems [21]. Absorption refrigeration cycles, in particular, harness thermal energy, including potentially that provided by PVT systems, to

drive the cooling cycle, thereby reducing the need for grid electricity [22]. By decreasing reliance on electricity to power mechanical compressors, these systems minimise environmental impact while also enhancing energy flexibility [21–23]. Previous studies have investigated the integration of absorption chillers for space cooling alongside PVT technologies in S-CCHP systems. For instance, Ramos et al. [24] studied hybrid PVT systems across ten European locations, showing that a 4–5 person, 100 m^2 home in Berlin could meet 100% of space cooling demand with 50 m^2 of PVT collectors and 80–90 °C water for the absorption chiller, whereas a similar home in Seville reached only 21%. Herrando et al. [25] evaluated S-CCHP systems with PVT collectors in the food-processing sector, noting environmental benefits but highlighting challenges such as long payback times compared to PV-only systems. Monghasemi et al. [26] assessed a solar absorption cooling system for a restaurant in Sweden, integrating PVT collectors, a storage tank, a single-effect absorption chiller, an auxiliary heater, and a cooling tower. The system met cooling demand while supplying ample hot water, with PVT collectors more cost-effective than traditional solar thermal collectors. Despite occasional deviations during peak cooling periods, surplus electricity supported chiller operation, achieving an average thermal efficiency of 28% and electrical efficiency of 6%. Furthermore, a recent study by Ghaith et al. investigated a concentrating-type PVT system coupled with a conventional absorption refrigeration unit for residential applications. The system was analysed for a 400 m^2 residential building and was able to supply approximately 60% of the cooling demand. The results showed a payback period of 3.12 years and annual CO_2 emission reductions of 461 tCO_2/year [19]. A review by Jiao et al. [27] highlighted persistent challenges for solar cooling systems using PVT, including limited prototype testing and scarce operational data, yet showed promising outcomes, e.g., absorption systems reaching a maximum COP of 0.615 with a minimum payback of 9.3 years, and adsorptive systems yielding up to 81.7 kWh/day with a maximum COP of 2.1 and a minimum payback of 8.45 years. These results underline the potential of thermally-driven solar cooling systems and the need for continued research to fully exploit them.

Although prior studies have explored thermodynamic models of PVT hybrid systems, mainly coupled with conventional absorption refrigeration, there remains a need for configurations that maximise both thermal and electrical outputs [12,13,28,29]. This need is particularly relevant in residential settings with limited rooftop space [12,27,28]. In this context, diffusion absorption refrigeration (DAR) emerges as a promising yet under-explored alternative. As a fully thermally-driven single-pressure absorption system [30], DAR enables electricity-free cooling, reducing grid stress during peak demand [21,31], and increasing operational flexibility by allowing more electricity to be exported, stored, or used within the household. DAR also offers other advantages over conventional absorption chillers, including no moving parts, lower maintenance requirements, extended operational lifetime, and compact, single-unit designs [21,30]. Its main limitation is the high operating temperature (typically above 100 °C), which often requires external heaters and can reduce efficiency; however, increasing efforts are being directed towards lowering this threshold [30,32]. Despite its potential, and although PVT systems have been extensively investigated in combination with heat pumps, conventional absorption chillers, and thermal storage [12,13,15,30,33–35], the integration of DAR with PVT collectors in residential S-CCHP systems remains largely unexplored [36]. To date, only a recent study has examined the potential integration of DAR with PVT systems across different climatic conditions, reporting promising performance particularly in regions with relatively low cooling demand [30]. This research gap is especially relevant given that space cooling is the primary driver of increasing energy demand in residential buildings, with global growth rates of approximately 4% per year [37]. Moreover, this study is, to the authors' knowledge, the only one that evaluates DAR-based cooling under realistic operating conditions, using hourly meteorological data and time-resolved residential energy demand profiles over an entire year [30]. However, the analysis does not explore system-level performance, as it is focused in a high-level comparison of different cooling technologies across climatic regions, thereby constraining the applicability of its conclusions for detailed system design and optimisation. A deeper understanding of this integration is therefore essential to establish the performance limits of fully thermally-driven cooling coupled with advanced solar technologies, and to support informed early-stage design decisions prior to undertaking costly experimental campaigns or pilot-scale deployments.

To address this critical knowledge gap, this study proposes a novel PVT-based S-CCHP system integrated with a DAR cycle, evaluating its technical feasibility alongside its economic and environmental performance. The work sets a precedent for future research on DAR–solar integration by considering fully coupled residential energy demands, including electricity, hot water, space heating, and cooling, under a low cooling demand scenario, providing detailed insights into the system's ability to meet energy needs, while maintaining representativeness through the use of hourly real-weather data and time-resolved residential demand profiles. For this purpose, a novel transient thermodynamic modelling framework is developed and numerically validated, combining open-source performance data from commercially available PVT systems with an experimentally validated DAR model based on [38]. The framework also enables the assessment of specific refrigerant–absorbent combinations within the DAR cycle, here applied to a low-GWP organic pair, supporting future identification of optimal working pairs from both economic and environmental perspectives. A direct comparison with PV- and ST-based systems is also carried out, using a rooftop utilisation factor derived from multiple sources, to benchmark the DAR–PVT configuration against typical residential use cases and explicitly account for rooftop constraints. In addition, a sensitivity analysis on the inclusion of battery storage and the trade-off between electricity export and self-consumption is performed. This aspect is particularly relevant given that the DAR cooling subsystem requires virtually no electricity to operate, fundamentally altering the conventional role of storage in solar-driven cooling systems. Finally, the developed model provides a robust foundation for further refinement in this largely unexplored research area, offering practical pathways for system optimisation, exploration of alternative working fluid pairs, and integrated assessment of techno-economic and environmental performance in DAR-based residential cooling systems.

2. Methodology

The study presents a novel PVT–DAR system modelled in MATLAB, integrating techno-economic and environmental parameters through a transient, hourly simulation of building energy demand and ambient conditions over an entire year. Primary outputs of this model include coverage ratios and energy requirements for residential purposes, specifically electricity for appliances and lighting, space heating (SH), residential hot water (HW), and SC. These outputs are essential for rigorous analysis to assess the economic viability and environmental implications of the system in the residential sector. While the model primarily focuses on PVT systems, a comparative examination with solar thermal (ST) and PV configurations is conducted to provide insights into potential improvements and to delineate the comparative merits and limitations of PVT technology. A comparison of DAR performance with other available cooling technologies is not undertaken at this stage due to the novelty of the proposed system with DAR integration, with system improvements planned to enable a more meaningful comparison with conventional air-conditioning systems in future work.

The thermodynamic model relies on detailed energy conservation and heat transfer equations governing the various subsystems within the S-CCHP system. Empirically derived equations are used to reduce idealisations, although experimental validation is still required to confirm the results obtained in this study. In terms of the economic

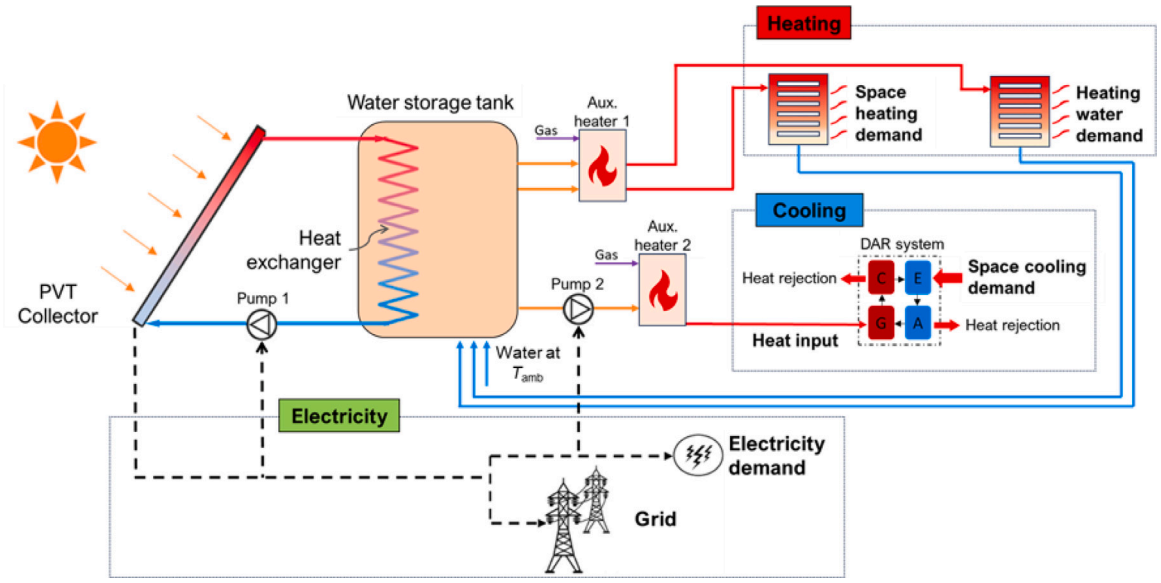

Fig. 1. Proposed system layout for solar combined cooling, heating and power based on PVT collectors.

and environmental performance, the model incorporates key energy market variables, including gas price, electricity tariffs, and the emissions factor of the German grid (i.e., the amount of CO_2-eq emitted per unit of electricity generated). This allows for the calculation of essential performance indicators such as the net present value (NPV), the payback time (PBT), and the avoided emissions associated with the proposed system deployment. Additionally, considering the critical role of rooftop space availability in system sizing, we conducted an extensive literature review to mitigate the risk of overestimating or underestimating the system's energy generation potential. The subsequent subsections provide further insights into these aspects.

2.1. System description

The system, shown in Fig. 1, comprises a PVT-based solar configuration, with the collectors producing both electricity and hot water simultaneously. The hot water, generated during PV-cell cooling, flows through pipes to a coil-type heat exchanger, transferring heat to water in a storage tank. The inclusion of a water tank stabilises hot water temperature fluctuations by leveraging water's heat storage capacity [39]. This stored water is then routed through separate circuits to the demand-side heat exchangers, supplying SH, HW, and the thermally-driven DAR unit. The system also includes two auxiliary gas-fired water heaters: one to raise the water temperature to meet the minimum thresholds for SH and HW demands, and the other to provide the additional thermal input required by the thermally-driven DAR unit to satisfy the total SC demand, considering that water tank temperatures may not reach the levels needed [24,40–42]. Electricity generated by the system is assumed to cover the demand of internal pumps, household appliances, and lighting, with no batteries included in the hourly analysis to simplify this system-level study. Excess electricity is exported to the grid, while grid power is imported during periods of insufficient solar generation.

To provide pragmatic insights into the feasibility of the proposed PVT-DAR system for residential demand, the selection of an appropriate PVT technology is crucial. Guided by market readiness and data availability, four commercially available flat-plate covered and uncovered water-based PVT collectors were identified and are summarised in Table 1, with their basic configurations illustrated in Figures 17 and 18 of [12], to which the reader is referred for detailed visualisation and working mechanisms. Considering their thermal and electrical efficiencies, PVT-2 and PVT-3, despite higher electrical efficiency, exhibit lower thermal efficiency, which increases the heat requirements for the absorption system, while PVT-4, although having the highest thermal efficiency, shows the lowest electrical efficiency. PVT-1, in contrast, shows intermediate values for both efficiencies. Moreover, PVT-1 is widely cited in system-level studies examining optimal tank-to-collector ratios ($V_{wt}/A_{c,total}$) and recommended mass flow rates [43–46], allowing the use of previous research insights for system optimisation in this study. Consequently, PVT-1 provides a balanced solution between thermal and electrical efficiency, suitable for residential demand types, while also enabling the application of established optimisation strategies from prior studies. The specific values applied in the model are a flow rate of 70 L/h per collector and an optimal $V_{wt}/A_{c,total}$ ratio of 50 L/m^2 [41,43], which, based on the total collector area calculated later in this study, corresponds to a water tank volume of 1.66 m^3.

For cooling, DAR units only utilise excess heat during peak cooling periods and therefore do not require electricity to power a compressor or pump. These units consist of four major components—the generator, condenser, evaporator and absorber [57]. The process begins in the generator, where residual heat from the PVT system causes a refrigerant-rich solution to boil ($\dot{Q}_{gen}$), while a bubble pump lifts the solution and separates refrigerant vapour from the liquid. The vapour passes through the condenser, where it rejects heat to the environment and condenses, before entering the evaporator, where it absorbs heat from the space to be cooled and evaporates. To reinitiate the cycle, the vapour enters the absorber, where the refrigerant is absorbed into a solution containing an auxiliary gas, which lowers the refrigerant partial pressure to enable evaporation at varying temperatures and drives its own circulation due to density differences caused by refrigerant concentration and temperature gradients [58]. Therefore, the cooling capacity of the DAR is defined by the heat absorbed in the evaporator. The thermodynamic complexity of DAR processes introduces various forms of heat loss, reducing the COP to 0.1–0.3 [21,31,59], depending on the refrigerant–absorbent pair and design choices.

The comparison between PVT, PV, and ST systems is conducted considering the same residential floor area and rooftop utilisation factor for all systems. The PV-based system consists of polycrystalline silicon cells rated at 240 Wp, with an electrical efficiency of 0.147 and a temperature coefficient of 0.0045, at an average cost of €228 per panel [41], without battery integration and excluding provisions for SH, HW, or SC, resulting in a total installed capacity of 5.3 kWp. The ST-based system uses evacuated tube collectors with an optical efficiency of 0.768, a first-order heat loss coefficient of 1.36, and a

Table 1
Summary of commercially available PVT collectors analysed to guide the selection for this study, based on key technical parameters. Data sources include manufacturer datasheets and literature under standardised conditions [47–50], prices [51–55], and volume flow estimates [43–45,56]. Abbreviations: Mono-Si = monocrystalline silicon PV cells; L/h·c = litres per hour per collector; FP cov./uncov. = flat-plate covered/uncovered; a_1, a_2 = heat loss coefficients; T_{ref} = Reference temperature; Wp = Watt-peak; β = Power temperature coefficient; Price in euros per collector.

Category	Parameter	Unit	PVT-1 [47]	PVT-2 [48]	PVT-3 [49]	PVT-4 [50]
General data	PVT type	–	FP cov.	FP uncov.	FP cov.	FP cov.
	Aperture Area	m^2	1.55	1.55	1.65	1.58
	Price	€/c	671	449	528	513
	Volume Flow	L/h·c	30–90	30–90	No Data	90–150
Electrical	Cell type	–	Mono-Si	Mono-Si	Mono-Si	Mono-Si
	η_{elec}	%	15.98	18.44	16.8	15.3
	β	1/K	0.0047	0.0039	0.0041	0.0038
	T_{ref}	°C	25	25	25	25
	Power	Wp	260	300	280	250
Thermal	η_{th}	–	0.51	0.472	0.472	0.55
	a_1	W/m^2K	4.93	9.5	9.1	6.3
	a_2	W/m^2K^2	0.021	0.0	0.0	0.08

Table 2
Summary of the main technical parameters used for the PVT, ST, and PV systems analysed in this study.

Category	Parameter	Unit	PVT system [47]	ST system [41,60]	PV system [41]
General data	Type of collector	–	Flat-plate	Evacuated tube	PV panels
	Aperture area	m^2	1.55	2	1.55
	Price	€/c	671	450 [61]	228
Thermal	η_{th}	–	0.51	0.768	–
	a_1	W/m^2K	4.93	1.36	–
	a_2	W/m^2K^2	0.021	0.0053	–
	Volume flow	L/h·c	70	120	–
	$V_{wt}/A_{c,total}$	L/m^2	50	50	–
Electrical	Cell type	–	Mono-Si	–	Poly-Si
	η_{elec}	%	15.98	–	14.7
	β	1/K	0.0047	–	0.0045
	T_{ref}	°C	25	–	25
	Power	Wp	260	–	240

second-order heat loss coefficient of 0.0053 [41,60], providing only SH and HW, following a layout similar to that of the PVT system, at an average cost of €450 per collector [61]. For clarity, the main technical parameters of the analysed solar technologies (PVT, ST, and PV) are summarised in Table 2.

2.2. System modelling

The model framework is carefully designed to simplify the complex energy dynamics of the physical system. This is achieved through a set of carefully selected equations to capture the essential aspects within the defined subsystems. These equations predict coverage ratios for various residential energy needs. The mathematical formulation draws upon established solar industry standards, empirical heat transfer models, and basic principles of thermodynamic energy analysis. Together, these elements constitute the core of the model. In the following subsections, we provide a detailed description of the mathematical framework.

2.2.1. Mathematical model

The mathematical model used for the system is built upon several assumptions aimed at simplifying calculations and speeding up hourly numerical resolution throughout the entire year. Five distinct subsystems are utilised to describe in detail the equations governing the physical aspects of the system: the PVT collector, water storage tank, SH heat exchanger, HW heat exchanger, and SC system. Modelling of the gas water heater for SH and HW demands is excluded, assuming its existing installation. The associated non-renewable gas consumption is directly incorporated into the economic and environmental assessment, assuming that the efficiency of the two gas-fired heaters aligns with that of commercial gas water heaters.

The equations governing the outputs obtained from the PVT collectors include the electrical and thermal efficiency equations. The electrical efficiency is described using the adapted Heydenreich efficiency equation [62], given by:

$$\eta_{MPP}(T_{mod}) = \eta_{MPP}(T_{ref})[1 + \beta(T_{mod} - T_{ref})], \quad (1)$$

where the electrical efficiency of the module at the maximum power point (η_{MPP}), at a given operating temperature (T_{mod}), is calculated as a function of the cell's temperature deviation from the efficiency at standardised irradiance and temperature reference conditions (G_{ref} = 1000 W/m^2 and T_{ref} = 25 °C). This calculation utilises the temperature coefficient of maximum power point (β), also known just as temperature coefficient, obtained from the manufacturer's data.

The optical, or thermal, efficiency (η_{th}), shown in Eq. (2), is mathematically defined as the ratio of the useful thermal power extracted (q_u'') to the incident irradiance (G_i), expressed using a polynomial correlation typically involving coefficients up to the second order. These coefficients are termed the optical efficiency (η_0), first-order heat loss coefficient (a_1), and second-order heat loss coefficient (a_2). The equation is usually presented with the reduced temperature (T_r), defined as $T_r = (T_{mf} - T_{amb})/G_i$. The thermal efficiency of a PVT collector is experimentally determined using methods akin to those employed for ST collectors, with the ISO method being the standard adopted by several European companies [63]. This method involves testing the collector under steady-state conditions, utilising the temperature difference between the mean fluid temperature, T_{mf}, and the ambient temperature, T_{amb} [64]. The mean fluid temperature is calculated as the average of the inlet and outlet temperatures of the PVT, $T_{mf} = (T_{PVT,out} + T_{PVT,in})/2$.

$$\eta_{th} = \frac{q_u''}{G_i} = \eta_0 - a_1 T_r - a_2 G_i T_r^2 \quad (2)$$

In the proposed model of the ISO method, an ideal heat exchange assumption is made for the PVT, as expressed by:

$$\dot{Q}_u = q''_u A_{c,total} = \eta_{th} G_i A_{c,total} = N_c \dot{m}_{fu} c_{p,water} (T_{PVT,out} - T_{PVT,in}) \quad (3)$$

Here, $\dot{Q}_u$ and q''_u represent the absorbed heat from solar energy in W and the absorbed solar heat flux in W/m^2, respectively, while $A_{c,total}$ is the total area of collectors, $\dot{m}_{fu}$ is the mass flow of water circulating through each of the PVT collectors and N_c the total number of collectors.

The water storage tank energy balance is underpinned by assumptions of perfect mixing, which eliminates spatial gradients in the water's physical envelope, allowing the temperature to be solely dependent on time ($T = f(t)$), and a constant total mass of water, ensuring that the outflowing water is promptly replaced by an inflow of water at an equivalent mass flow rate [43]. Then, the energy balance of the water storage tank can be written as:

$$M_{wt} c_{p,water} \frac{dT_{wt}}{dt} = \dot{Q}_{PVT\to wt} + \dot{Q}_{sh} + \dot{Q}_{hw} + \dot{Q}_{loss} + \dot{Q}_{sc\to gen} \quad (4)$$

The left term of the equation represents the energy accumulation in the water stored in the tank. Here, M_{wt} denotes the total mass of water inside the storage tank, $c_{p,water}$ stands for the heat capacity of water, and dT_{wt}/dt represents the rate of change in the tank water temperature over time. The equations used to calculate the power consumption of the pumps are reported in Appendix A.

The heat transfer from the PVT circuit water to the stored water, denoted as $\dot{Q}_{PVT\to wt}$, is computed as the difference between the inlet energy flow of heated water from the PVT and the outlet energy flow of water leaving the tank to the PVT, facilitated by a coil-type heat exchanger, which is modelled using the Effectiveness-Number of Transfer Units (ε-NTU) method [65]:

$$\dot{Q}_{PVT\to wt} = \varepsilon_{coil} c_{p,water} \dot{m}_{fa} (T_{PVT,out} - T_{PVT,in}), \quad (5)$$

where, $\dot{m}_{fa}$ signifies the mass flow rate of water circulating inside the coil. Here, the effectiveness ε is determined as a function of the number of transfer units (NTU). The correlations and details of the heat transfer equations governing the coil and water tank are presented in Appendix B.

The second and third terms in Eq. (4) represent the energy allocated for SH and HW demand ($\dot{Q}_{sh\,or\,hw}$). This allocation is based on the assumption of minimum required temperatures on the demand side and the availability of water in the tank at the same temperature level, as defined by the following conditions:

$$\dot{Q}_{sh,cov\,or\,hw,cov} = \begin{cases} \dot{Q}_{dem}, & \text{if } T_{wt} \geq T_{feed} \\ \dot{m}_{dem} c_{p,water} (T_{wt} - T_{in}), & \text{if } T_{wt} < T_{feed} \\ 0, & \text{if } T_{wt} \leq T_{in} \end{cases} \quad (6)$$

Here, $\dot{m}_{dem}$ represents the circulating mass flow of water for the SH or HW circuits. The minimum common temperatures required for the service temperature, T_{feed}, are set at 60 °C and 45 °C for SH and HW, respectively, while the inlet temperatures of the water to be heated, T_{in}, are assumed to be 30 °C and 10 °C [66].

Heat losses are exclusively accounted for in the water storage tank, under the assumption of ideal insulation in pipes and other system elements. These losses are modelled by considering them as a function of the external surface area of the tank, the overall heat transfer coefficient of losses, and the temperature difference between the water stored in the tank and the ambient temperature, as expressed by the equation:

$$\dot{Q}_{loss} = U_{wt} A_{wt} (T_{amb} - T_{wt}) \quad (7)$$

Here, A_{wt} denotes the external surface area of the storage tank, while U_{wt} represents the overall heat transfer coefficient.

Similar to the SH and HW demand circuits, the energy allocated for the thermally-driven refrigeration unit, denoted as $\dot{Q}_{sc,gen}$, is determined as the difference between the energy entering the tank — originating from makeup water at ambient temperature — and the energy of the water leaving the tank toward the cooling system. It is worth noting that no return of the warm water used in the DAR unit is accounted for, to preserve this recirculation as a prospective area for further research. To provide a more detailed description, the SC provision system is modelled using four sub-models. The first sub-model addresses the thermodynamics and primary equations governing the DAR unit, described through a simplified lumped model. This involves approximating more intricate simulations through a reduced-order power model. For a given refrigerant-absorbent pair, the power model establishes a relationship between the required generator thermal power, generator, temperature, ambient temperature and cooling [38].

The first step involves reaching a minimum wall temperature on the generator to initiate the evaporation process of the refrigerant-absorbent pair. This minimum wall temperature (T_{gen}) is determined by:

$$T_{gen} = e\,(T_{amb})^p\,(\dot{Q}_{gen,exp})^g + j \quad (8)$$

Here, T_{amb} represents the ambient temperature, $\dot{Q}_{gen,exp}$ indicates the experimental input heat data, and e, p, g, j are empirical constants.

Next, the heat input required by the generator for continuous operation is calculated as:

$$\dot{Q}_{gen} = N_{DAR} \frac{\left[\upsilon\,(T_{amb})^x \left(\frac{\dot{Q}_{sc,dem}}{N_{DAR}}\right)^y + z\right](T_{sc} + 273.16)(T_{amb} - 5)}{278.16(T_{amb} - T_{sc})} \quad (9)$$

N_{DAR} represents the total number of DAR units connected in parallel. It is calculated as the number of units required to fully meet the SC demand, based on the nominal power of each unit, estimated using an empirical correlation with the maximum ambient temperature at the location, developed by one of the authors of this study, and assuming a COP of 0.3. $\dot{Q}_{gen}$ represents the minimum required heat input for all generators in the cooling system, $\dot{Q}_{sc,dem}$ signifies the SC demand for the region under study, T_{sc} denotes the desired cooling temperature to be achieved, and υ, x, y, z are empirical constants. A correction factor, akin to that described in [67], is applied to adjust for the experimental conditions where domestic fridges with 5 °C were used. Regarding the DAR model accuracy, the predictions show excellent agreement with experimental data for the generator wall temperature (AAD = 0.53%, Eq. (8)) and a higher but acceptable deviation for the cooling rate (AAD = 30%, Eq. (9)), which is considered suitable for this system-level performance assessment. Further details, including error analysis, are provided in Appendix C.

The following sub-model describes the heat exchanger that supplies the required heat to the DAR generator. The mathematical framework employed is the ε-NTU model, as detailed in [68], owing to the unknown inlet and outlet temperatures from the generator heat exchanger:

$$\varepsilon_{gen} = \frac{T_{in,hot} - T_{out,hot}}{T_{in,hot} - T_{gen}}, \text{then}: \quad T_{in,hot} = \frac{T_{out,hot} - T_{gen}\varepsilon_{gen}}{1 - \varepsilon_{gen}}, \quad (10)$$

where $T_{in,hot}$ and $T_{out,hot}$ represent the inlet and outlet temperatures, respectively, of the water from the generator's heat exchanger originating in the water tank.

The effectiveness (ε_{gen}) is subsequently determined as a function of the Number of Transfer Units using the equations:

$$\varepsilon_{gen} = 1 - e^{(-NTU_{gen})}, \text{ and} \quad (11)$$

$$NTU_{gen} = \frac{UA}{c_{p,water}\dot{m}_{sc,cov}}, \quad (12)$$

where $\dot{m}_{sc,cov}$ denotes the mass flow rate of water circulating in the SC provision system and UA represents the product of the overall heat transfer coefficient and heat exchange area.

The calculation of NTU_{gen} requires experimental heat transfer data. Reviewing the DAR systems presented in [69], it is evident that the designs of generator heat exchangers vary widely. Despite extensive

research on DAR performance and thermodynamic parameters, scant information exists regarding experimental data on heat transfer properties for modelling a specific DAR generator operating with heated water. To address this gap, information from conventional absorption chillers is utilised as a benchmark for practical heat transfer values relevant to the generator's heat input. Among four papers reviewed [70–73], only one provides the necessary thermodynamic data for this model. As a result, the parameters outlined in [70] form the basis for the numerical computations in MATLAB. Despite the use of LiBr/H_2O as the working pair in that investigation, the estimated effectiveness provides a benchmark for the thermodynamic performance of the generator's heat exchanger within the DAR unit.

Another consideration is that, given the unknown design temperatures, the Exchanger Minimum Approach Temperature (EMAT) method is employed to estimate $T_{out,hot}$, with a T_{min} set to 5 °C, as recommended for refrigerants [74]. Once the inlet and outlet temperatures are calculated, the mass flow required for the DAR generators is determined, considering the influence of the total required number of DAR units N_{DAR}, by:

$$\dot{m}_{sc,cov} = \frac{\dot{Q}_{gen}}{c_{p,water}(T_{in,hot} - T_{out,hot})} \tag{13}$$

The auxiliary water heater is crucial for providing additional heat to achieve the required temperature level for the generator. This auxiliary heater, assumed to operate under ideal conditions, is utilised to calculate the additional heat input necessary for the DAR units to meet the entire SC demand, regardless of whether the required energy is supplied by gas-fired or electrical heaters:

$$\dot{Q}_{heater} = \dot{m}_{sc,cov} c_{p,water}(T_{in,hot} - T_{wt}) \tag{14}$$

The fourth and final sub-model describes the heat transfer from the DAR unit to the designated space requiring cooling. It assumes that cooling is either fully provided or not provided, with no consideration for partial coverage scenarios. This is expressed mathematically as:

$$\dot{Q}_{sc,cov} = \dot{Q}_{sc,dem}, \quad \text{for all times when } \dot{Q}_{sc,dem} > 0 \text{ and } T_{amb} > T_{sc}, \tag{15}$$

where T_{sc} represents the set temperature for SC (18 °C).

The aforementioned equations form a coupled system in which the key thermodynamic variables must be determined. The differential equation governing the water tank dynamics is solved using the implicit Backward Euler method, while a fixed-point iterative procedure is employed at each hourly time step. This iterative approach is adopted because certain heat transfer parameters, such as those of the coil-type heat exchanger, are temperature-dependent and must therefore be estimated and updated iteratively within each time step. The proposed model is validated numerically, as detailed in Appendix D. Stable convergence occurs for over 99.85% of time steps, with the fixed-point iteration requiring on average 5.74 steps (90th and 99th percentiles: 18 and 26). Absolute errors for converged steps remain well below the $1 \cdot 10^{-5}$ °C tolerance, averaging $2.71 \cdot 10^{-6}$ °C (90th: $7.70 \cdot 10^{-6}$ °C, 99th: $9.72 \cdot 10^{-6}$ °C). The 13 non-converged steps (0.15%) exhibit low-amplitude oscillations (0.1 °C) with negligible effect on annual performance, confirming the method's convergence, accuracy and stability. Additional validation is carried out by comparing the simulated results, particularly the predicted temperatures, with those reported in previous studies [24,25,40,41,43], thereby confirming the suitability of the adopted numerical methodology. Although experimental validation of the proposed system is left for future work, the present system-level modelling and solution strategy provides a robust framework for identifying key parameters and design considerations to guide subsequent experimental investigations.

2.3. Economic and environmental performance indicators

The economic model implemented in this study computes annualised economic outcomes by leveraging variables outlined in previous works [24,41,43]. It is noteworthy, as elucidated in [75,76], that employing the levelised cost of energy as equivalent electricity ($LCOE_{eqel}$) does not adequately assess investment viability. Consequently, the net present value (NPV) and the payback time (PBT) serve as primary reference indicators for economic performance evaluation. Table 3 summarises the main data used to estimate investments and costs within the model.

The cost savings achieved by implementing the proposed system, compared to a baseline scenario in which all energy demand is met through imported electricity and natural gas, are calculated as follows:

$$C_s = -C_{O\&M} + (E_{cov} + E_{sc,cov,eqel})c_e + E_{exc}s_e + \frac{(Q_{sh,cov} + Q_{hw,cov} - Q_{heater})c_{ng}}{\eta_{heater}}, \tag{16}$$

where, C_s denotes the cost savings, encompassing all savings realised through the operation of the PVT system to meet SH, HW, SC, and electricity demands.

The profits generated by implementing the PVT-based system stem from several sources: covering electrical demand (E_{cov}) at a given cost of electricity from the grid (c_e), selling excess electricity to the grid (E_{exc}) at a specified selling price (s_e), and meeting SH and HW demand ($Q_{sh,cov}, Q_{hw,cov}$) at a predetermined cost of natural gas (c_{ng}). The natural gas-fired heaters are assumed to operate with an efficiency (η_{heater}) of 82%. Additionally, savings are also accounted for by covering SC demand ($E_{sc,cov,eqel}$) at a given cost of electricity from the grid. Inverter losses are not explicitly included in this system-level analysis, as they are typically minor and relatively consistent across rooftop PV applications. Reported inverter efficiencies in the literature range from 95% to 98.5%, depending on factors such as inverter load, ambient temperature, and system design, which correspond to conversion losses of approximately 1.5% to 5% [81–83]. While these losses have been neglected in this study to maintain a broader system perspective, they can be incorporated in future work to enhance the precision of performance estimates.

The operating costs of the auxiliary water heater for the operation of the DAR units (Q_{heater}) at a given c_{ng} and the operation and maintenance costs ($C_{O\&M}$) are subtracted from the generated profits. The $C_{O\&M}$ are set at 1% of the total system investment [41]. Pump calculations are also employed to estimate investment costs; however, their operating costs are minor and have negligible impact on the system's electrical performance. Consequently, they are included within the overall electrical appliances demand.

Cost savings facilitate the calculation of both NPV and PBT of the system, as expressed in Eqs. (17) and (18):

$$NPV = -I_o + \frac{C_s}{(d - i_f)}\left[1 - \left(\frac{1 + i_f}{1 + d}\right)^n\right], \text{ and} \tag{17}$$

$$PBT = \frac{\ln\left[\frac{I_o(i_f - d)}{C_s} + 1\right]}{\ln\left(\frac{1+i_f}{1+d}\right)} \tag{18}$$

Here, I_o represents the total initial investment covering various expenditures (PVT collectors, DAR units, auxiliary heater, among others), d denotes the discount rate, i_f signifies the inflation rate, and n is the investment horizon (assumed to be 25 years).

Regarding the environmental performance of the proposed system, since this study focuses on the residential sector, the cost of emitted CO_2-eq is not presently considered. Therefore, only the annual avoided emissions of CO_2-eq are used as a metric to measure performance, which are calculated according to Eq. (19). Nonetheless, as

Table 3
Component investment costs for PVT S-CCHP, PV, and ST systems analysed.

System	Component	Value	Unit	Source
PVT S-CCHP	PVT Collector	671	€	[47]
	Mounting	59	€/collector	[41]
	System installation	40	€/m^2	[41]
	DAR unit	684	€	[38]
	Auxiliary heater	3000	€	[77–79]
	$C_{O\&M}$	$0.01I_o$	€	[41]
ST System	ST Collector	450	€	[61]
	Mounting	47.2	€/collector	[41]
	System installation	24	€/m^2	[41]
	$C_{O\&M}$	$0.01I_o$	€	[41]
PVT/ST Thermal System	Water storage tank	$0.874V_{wt} + 763.5$	€	[43]
	Heat transfer fluid	3.3	€/L	[41]
	Piping	$(0.897 + 0.21d_{pipe})L_{pipe}$	€	[80]
	Pump station	265	€	[43]
	Controller	110	€	[43]
	Expansion vessel	140	€	[41]
	Pumps	$500(\dot{W}_{pump}/300)^{0.25}$	€	[80]
PV System	PV Panel	950	€/kWp	[41]
	$C_{O\&M}$	$0.01I_o$	€	[41]

Table 4
Summary of key location-specific input parameters used in the model, including location, building, demand, and economic and environmental data.

Category	Parameter	Notes
Location	City	Berlin, Germany. Representative urban context with seasonal energy demand.
Building	Dwelling area	83 m^2. Average single-family home in Germany [85].
	Rooftop utilisation factor	0.4. Average from multiple sources [86–96].
	Collectors covered area	33.2 m^2. Identical for the PVT, ST and PV systems.
Thermal demand	Load profile	Hotmaps database. Includes SH, SC, and HW as UED and FEC [97].
	Annual demand	Hotmaps database. Includes SH, SC, and HW as UED and FEC [97].
	Indicator used	UED. Net energy required to cover the SH, SC, and HW demand.
Electricity demand	Load profile	Hotmaps database [97].
	Annual demand	Electricity demand for appliances and lighting, excluding SH, HW and SC [98].
Ambient data	Irradiance	PVGIS-SARAH2 database. Inclined plane; normalised to obtain hourly profile [99].
	Temperature profile	PVGIS-SARAH2 database. 2-meter air temperature [99].
Economic-environmental	See Table 5	Includes energy prices, discount rate, CO_2-eq factor, inflation.

cited in [84], the real estate sector is anticipated to be subject to carbon pricing in the future.

$$AE_{av} = (E_{cov} + E_{sc,cov,eqel} + E_{exc}) f_{elec} + \frac{(Q_{sh,cov} + Q_{hw,cov} - Q_{heater}) f_{ng}}{\eta_{heater}} \quad (19)$$

Here, AE_{av} denotes the annual avoided emissions in kilograms of CO_2-eq, f_{elec} represents the German grid emission factor, and f_{ng} represents the natural gas emission factor, both provided in Table 5.

2.4. Data collection and processing

This section summarises the key location-specific data inputs used in the model, including building characteristics, energy demands, and economic-environmental parameters. Table 4 provides a concise overview of these inputs. Specific details related to the table are described throughout this section.

2.4.1. Location

Berlin, the capital of Germany, is selected as the case study due to its strategic relevance for assessing solar energy systems in European urban contexts, with over 560,000 buildings and potential to install solar systems on 25% of them [100]. Its seasonal energy demand, characterised by high SH in winter and moderate SC in summer, makes it suitable for evaluating integrated PVT and thermally-driven refrigeration systems, as its relatively low cooling demand compared to southern European locations, combined with sufficiently high summer solar irradiation, provides favourable operating conditions for DAR-based thermally-driven refrigeration systems by limiting reliance on the auxiliary heater [30]. Recent policy incentives, such as the removal of sales tax on solar modules since 2023 [101], further support solar adoption. Additionally, the findings obtained for Berlin provide valuable insights for similar temperate urban areas with seasonal heating dominance and moderate cooling (e.g., Vienna, Paris, Warsaw, Toronto), and the methodology used can be adapted to other climatic or policy contexts.

2.4.2. Building, macroeconomic and environmental data

The total area of the residential building considered in this study corresponds to the average size of a single-family dwelling in Germany, 83 m^2, as reported in [85]. Equally important is the actual area available to be occupied by the collectors, which is determined by the rooftop utilisation factor. A comprehensive analysis, drawn from diverse sources [86–96], allows for the estimation of an average value of 0.4. The economic and environmental variables at the country level for Germany and their sources are summarised in Table 5.

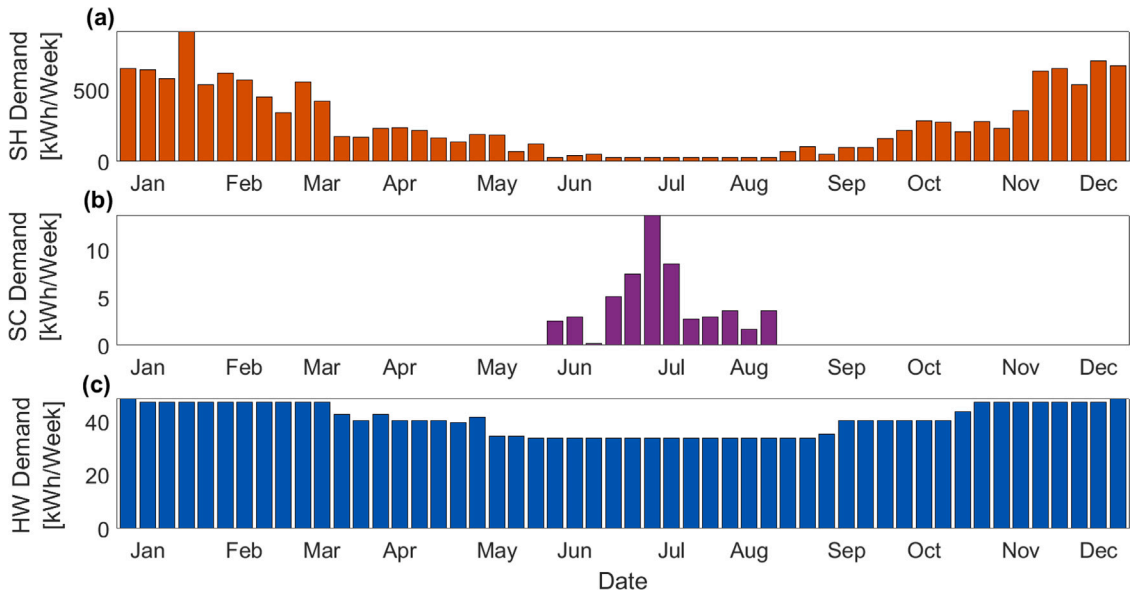

Fig. 2. Weekly energy demand for (a) space heating (SH), (b) space cooling (SC) and (c) hot water (HW) in a typical residential building of 83 m^2 in Berlin, Germany.

Table 5
Germany - Economic and emissions parameters (2023).

Variable	Value	Unit
Electricity purchase price [102]	0.2333	€/kWh
Electricity selling price [103]	0.1166	€/kWh
Natural gas price [104]	0.0741	€/kWh
Interannual inflation rate [105]	0.087	–
Discount rate [106]	0.0364	–
CO_2 emission factor of electricity [107]	0.38	$kgCO_2$-eq/kWh
CO_2 emission factor of natural gas [108]	0.201	$kgCO_2$-eq/kWh

2.4.3. Thermal energy demand

Thermal energy demand data for SH, SC, and HW are sourced from the Hotmaps project database [97], available at the NUTS2 spatial resolution [109]. This dataset includes total annual demand and normalised hourly demand profiles for 2010, provided as UED (Useful Energy Demand) and FEC (Final Energy Consumption). The discrepancy between UED and FEC arises from conversion factors that account for the efficiency of supply technologies, distribution losses, and user behaviour. For the purposes pursued in this study, UED is used as the objective is to measure the performance of the PVT-DAR system to cover the real demand.

Fig. 2 presents the weekly energy demand profiles over the course of a year for SH, HW, and SC. These profiles are obtained by summing the hourly values for each type of demand over every complete week. A marked seasonal contrast is observed: SH demand peaks during the winter months, while SC demand appears only in the warmer season and is absent in winter. In contrast, HW demand remains relatively stable throughout the year. The difference in magnitude between SH and SC is also notable, with SC staying below 15 kWh/week in summer, whereas SH regularly exceeding 350–400 kWh/week during winter.

2.4.4. Electricity demand

To address electricity demand, it is important to separate total annual consumption from the load profile. Since Hotmaps electricity data include SH, SC, and HW, total electricity demand excluding these components is obtained from [98], covering appliances — but not air conditioning — and lighting. Although data is only available for 2019, the 9-year gap is unlikely to affect estimates significantly, given Berlin's stable population growth from 3.44 million in 2010 to 3.64 million in 2019 [110]. The electricity load profile, sourced from Hotmaps (2010), reflects the entire electrical system rather than only residential use; nevertheless, it is used here for simplicity.

2.4.5. Ambient conditions

Irradiance and temperature profiles are sourced from the PVGIS-SARAH2 database [99], where irradiance is presented as global irradiance on an optimised inclined plane in W/m^2, while ambient temperature is provided as the 2-meter air temperature in °C. To ensure consistency with the Hotmaps database, these variables are selected for the year 2010. The MATLAB model employs a normalised irradiance profile and total irradiance per m^2 to calculate the hourly irradiance profile in Wh/m^2. Since PVGIS provides irradiance in W/m^2, the normalised irradiance profile is computed by dividing each hour's irradiance by the sum of all the irradiance values over the year.

3. Results and discussion

This section presents a detailed analysis of the system's performance under transient, monthly, and annual operating conditions. The impact of ambient conditions and solar irradiance on thermal and electrical outputs is examined, along with how these outputs satisfy the building's heating, cooling, and electricity demands throughout the year in Berlin. Furthermore, the system's coverage ratios are benchmarked against those of conventional ST and PV technologies to evaluate its overall efficiency and potential. The system evaluated corresponds to the configuration previously described and illustrated in Fig. 1.

3.1. Transient operation

In Fig. 3, the correlation between ambient temperature, total irradiance, and the resulting water tank temperature in Berlin is depicted, while employing normal butane (nC_4) as the refrigerant and normal octane (nC_8) as the absorbent for the DAR unit. A notable decrease in the water temperature stored in the tank is evident during months exhibiting a substantial decline in the total received irradiance in the PVT collector area. The attained water tank temperature throughout the year, as delineated in Eq. (6), governs the coverage ratio of SH and HW, and also determines the supplementary thermal input from the auxiliary heater necessary for the proper functioning of the DAR system.

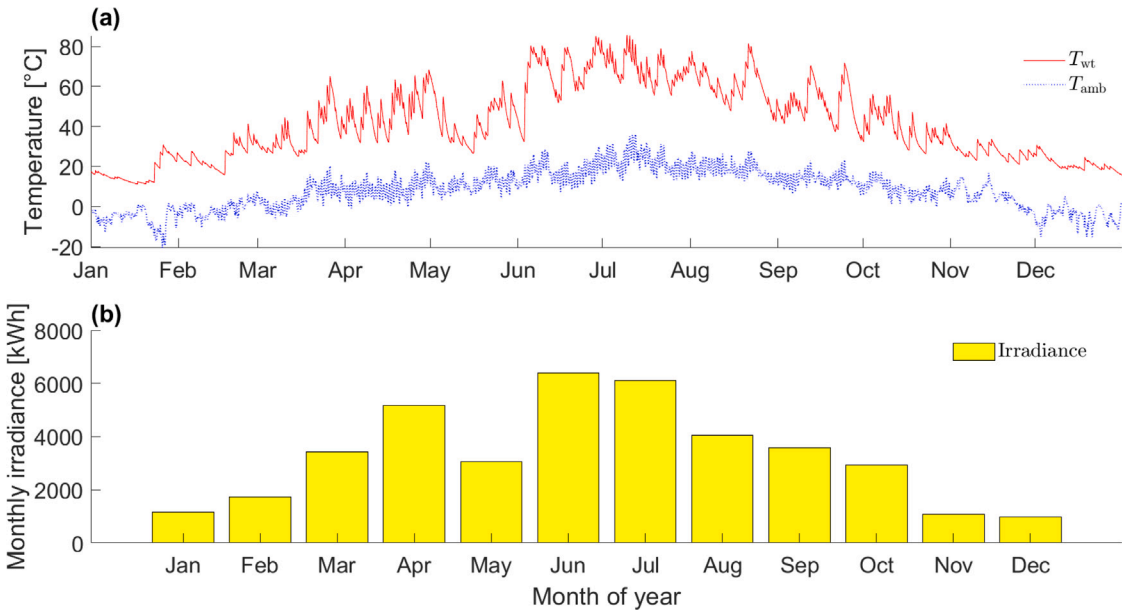

Fig. 3. (a) Influence of ambient temperature (T_{amb}) on the water tank temperature (T_{wt}) and (b) monthly solar irradiance, in Berlin over the full simulated year.

Following a comprehensive examination of the annual trend, we delve into the details of typical summer and winter weeks. The process of defining the typical week involved the application of specific criteria to identify peak demand periods. During winter analysis, the focus was on identifying the week with the highest mean demand for SH, selecting then the same weeks for SC and HW. Similarly, for typical summer weeks, priority was given to the week with the highest mean demand for SC, resulting in the selection of the same weeks for SH and HW. This systematic approach ensures consistency in assessing demand patterns across seasons and facilitates a focused analysis of energy consumption trends.

Results for a typical summer week are elucidated in Fig. 4. The SH demand is not depicted in this summer scenario as it is considerably lower than the SC demand during warm months. It can be distinctly seen in Fig. 4(a) that the SC demand is adequately met; however, the additional thermal input from the auxiliary heater significantly surpasses the minimum generator heat input requirement. This discrepancy can be attributed to the model's assumption that water tank replenishment occurs by replacing the outflow with inflow of water at ambient temperature. Despite the inherent inefficiency associated with this assumption, its retention serves the purpose of investigating potential enhancements to the DAR system proposed in this study. Exploring the potential for recirculating the discharged hot water from the DAR units stands as a promising avenue for further investigation in heat recovery optimisation.

Additionally, it is noteworthy to correlate, during the typical summer week, the extra thermal input required for the DAR system with the temperature differential between the water in the tank and the minimum temperature necessary at the generator's wall. Even during summer months characterised by high irradiance levels, the water tank temperature (T_{wt}) fails to reach the minimum temperature threshold required for the generator's wall with the nC$_4$-nC$_8$ refrigerant-absorbent. Typically, the temperature required for the generator (T_{gen}) exceeds 110 °C for this specific refrigerant-absorbent combination.

In Fig. 5, the typical profiles for a winter week in Berlin are presented. Given the negligible SC demand during colder months, only the thermal demands for SH and HW are depicted. As illustrated in Fig. 5(a), the hot water stored in the tank scarcely meets any of the SH demand. Conversely, depicted in Fig. 5(b), only a fraction of the HW demand is satisfied. This shortfall can be attributed to the fact that the minimum temperatures required for coverage exceed the water tank temperature. This disparity arises from lower irradiance levels during winter months and increased heat loss to the environment due to colder ambient temperatures. However, as noted in the system modelling, any demand not met by solar energy from the PVT collectors is compensated by the auxiliary gas heater shown in Fig. 1.

Electricity generation during typical winter and summer weeks closely mirrors the irradiance profile. In winter, less pronounced peaks of generation are observed, a direct consequence of the reduced irradiance levels characteristic of the season. Consequently, surplus electricity production during a typical winter week is correspondingly lower compared to summer. Conversely, during summer, the higher irradiance levels compared to winter facilitate increased electricity generation and the production of surplus electricity. It is evident from both Figs. 4 and 5 that PVT power output adequately meets electricity demand solely during daylight hours.

3.2. Monthly operation

In Fig. 6, the demands, coverages, thermal requirements for the DAR system, and ambient conditions for Berlin are illustrated. The profiles for SH and HW demands are presented in Fig. 6(a) and (b), respectively. As deduced from the typical weekly profiles for summer and winter, the monthly profile spanning the entire year indicates that during winter months, the hot water within the tank fails to satisfactorily meet the SH demand, while the HW demand is only partially fulfilled. In contrast, during summer (June–August), both demands are nearly entirely satisfied.

Focusing the analysis on summer months, we examine the minimum energy requirements for the DAR system to fulfil the entire SC demand. As depicted in Fig. 6(c), the minimum thermal input required by the generator notably exceeds the household's SC demand, and the additional thermal input from the heater is significantly higher compared to both the SC demand and the generator's minimum requirements. As previously discussed, this scenario arises from the assumption that there is no recirculation of already warm water from the DAR unit back into the water tank, coupled with the considerable disparity between the achieved T_{wt} and the minimum T_{gen}. Consequently, there is substantial potential for improving heat recovery, and also further research on refrigerantabsorbent combinations that allow to reduce T_{gen}.

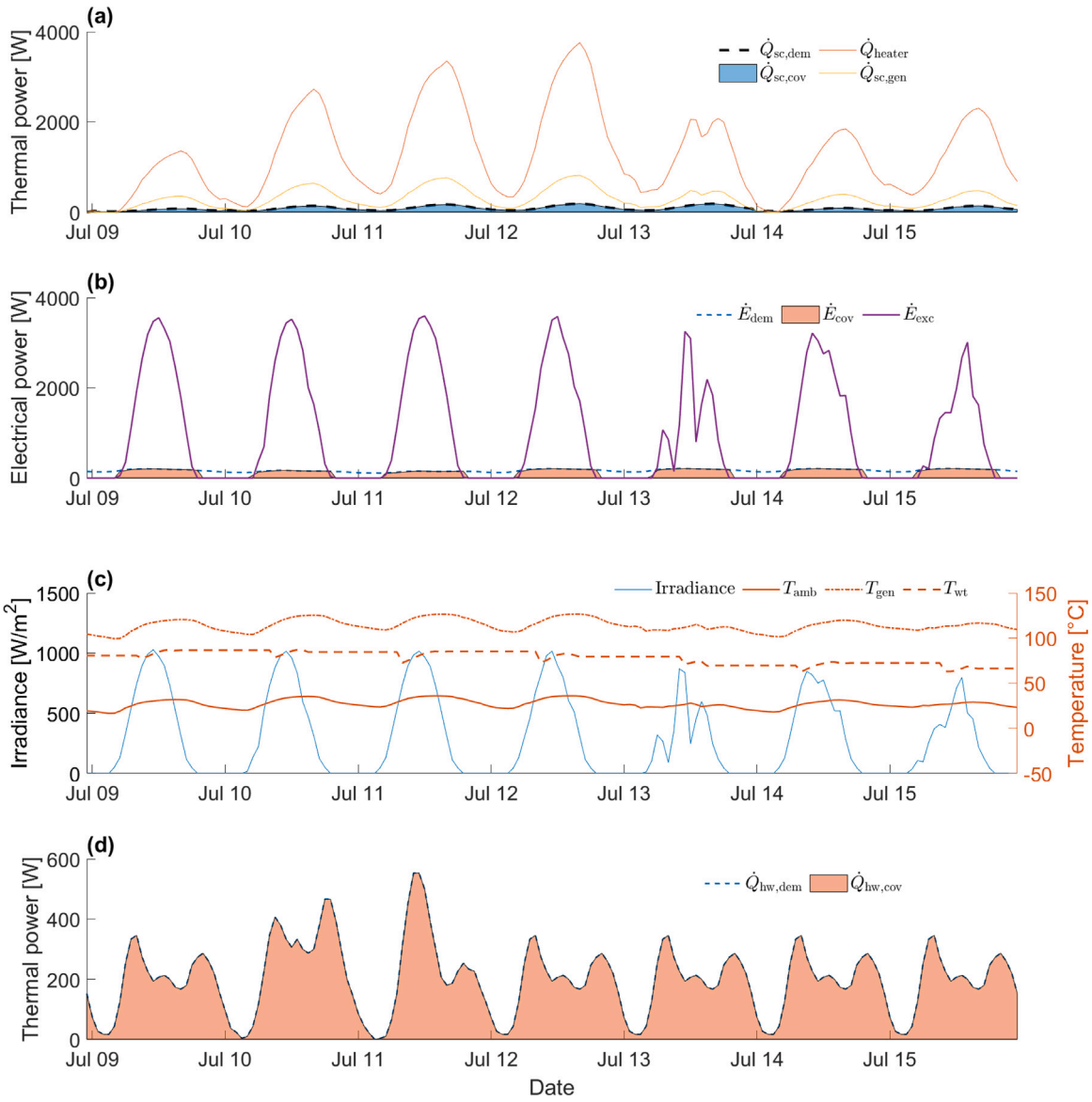

Fig. 4. Typical summer week profiles (July 9–July 15) in Berlin for (a) Space cooling demand ($\dot{Q}_{sc,dem}$) and covered cooling demand ($\dot{Q}_{sc,cov}$), auxiliary heater energy input ($\dot{Q}_{heater}$) and DAR generator minimum energy requirements ($\dot{Q}_{sc,gen}$); (b) electricity demand ($\dot{E}_{dem}$), covered electricity demand ($\dot{E}_{cov}$) and excess electricity ($\dot{E}_{exc}$); (c) irradiance, ambient temperature (T_{amb}), minimum DAR generator temperature requirement (T_{gen}) and achieved water tank temperature (T_{wt}).

For electricity generation, it is evident that only approximately 50% of the demand for appliances and lighting is met throughout the year. As previously mentioned, this shortfall is attributed to the absence of batteries in the proposed system. Instead, a significant surplus of electricity is produced, with peak values reaching up to 730 kWh during summer months. The model assumes that this surplus electricity is directly supplied to the grid. However, this raises the question of long-term storage for utilising this excess electricity during winter months, such as for operating a heat pump.

3.3. Yearly energy demand coverage ratios

The yearly performance of the proposed system is evaluated and compared with typical PV and ST based systems to assess its potential. The coverage ratio results are presented in Fig. 7. It is noteworthy that the proposed systems in neither case operate with batteries. In the ST-based system, the system layout resembles that shown previously in Fig. 1, with the exception that no SC is assumed to be covered, and no electricity generation occurs, as would be typical in a residential ST system. In the PV-based system, no SH, HW, or SC is assumed to be covered. Only electricity generation, coverage for appliances and lighting, as well as selling excess electricity to the grid, are considered. For both ST and PV systems, the same rooftop utilisation factor (0.4) and house's area (83 m^2) is assumed, with the total deployment of collectors or panels, respectively, in that available area.

The comparison of coverage ratios in Fig. 7 clearly reflects the aforementioned assumptions, with the ST scenario showing coverage for SH and HW, and the PV case providing coverage solely for electricity for appliances and lighting. For the PVT system, the yearly coverage ratios are 48% for electricity, 12% for SH, and 68% for HW, while SC, as per model assumptions, is assumed to be 100% covered by the DAR system. In contrast, with ST, higher SH and HW coverages are achieved, at 37% and 88%, respectively, while the PV-based system allows for 48% coverage of electricity for appliances and lighting, nearly identical to that of the PVT-based system. The disparity in SH and HW coverage ratio between PVT and ST arises from the fact that the latter is designed exclusively to attain higher temperatures, while the former pursues a compromised solution between thermal and power generation, considering that commonly used monocrystalline Si-cells deteriorate above

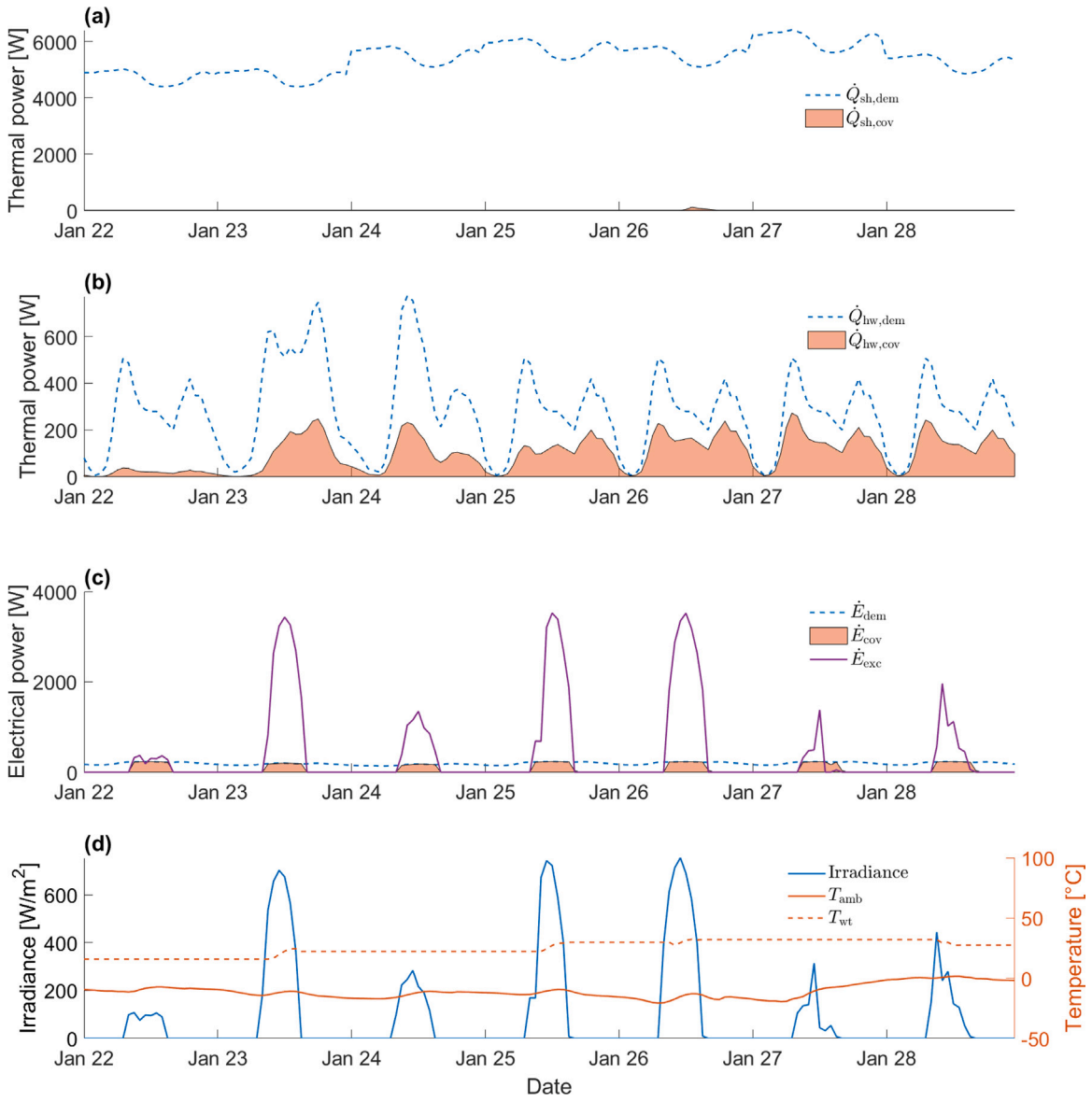

Fig. 5. Typical winter week profiles (January 22–January 28) in Berlin for (a) Space heating demand ($\dot{Q}_{sh,dem}$) and covered space heating demand ($\dot{Q}_{sh,cov}$); (b) hot water demand ($\dot{Q}_{hw,dem}$) and covered hot water demand ($\dot{Q}_{hw,cov}$); (c) electricity demand ($\dot{E}_{dem}$), covered electricity demand ($\dot{E}_{cov}$) and excess electricity ($\dot{E}_{exc}$); (d) irradiance, ambient temperature (T_{amb}) and water tank temperature (T_{wt}).

85 °C [111]. In terms of useful energy delivered on a collector-area basis, the PVT system provides 162.4 kWh/m^{2}åyear of electricity and 110.0 kWh/m^{2}åyear of thermal energy. For comparison, the PV system delivers 163.8 kWh/m^{2}åyear of electricity, while the ST system delivers 213.9 kWh/m^{2}åyear of thermal energy. It should be noted that, for the PVT system, all generated energy is considered useful: excess electricity can be exported, while the remaining electricity and thermal energy can always be used to meet residential demands. Moreover, the PVT system simultaneously covers SH, HW, and the thermal demand of the DAR system, whereas the ST system is assumed to meet only SH and HW needs, as indicated in Section 2.1. As a result, the PVT system provides a more balanced and higher total useful energy per unit area when all energy streams are considered.

3.4. Economic and environmental performance

This study evaluates the economic and environmental performance of the proposed PVT-DAR system, which operates in conjunction with auxiliary natural gas heating and imported electricity. The system is benchmarked against a baseline scenario in which the total energy demand is met exclusively through natural gas heating and grid electricity. The assessment is based on three primary indicators: net present value, payback time, and avoided carbon dioxide emissions. For comparative purposes, conventional PV and ST systems are also analysed under equivalent boundary conditions, whereby any unmet demand is likewise assumed to be supplied by natural gas heating and imported electricity from the grid. In Fig. 8(a), it is evident that the PVT-based system exhibits the least attractiveness, with an *NPV* of €7836, followed by the ST-based system at €11,265. Conversely, the PV system demonstrates the most favourable outcomes, boasting an *NPV* of €23,603. In Fig. 8(b) can be seen the *PBT* results, which mirrors the *NPV* results trend, with the PV system having the shortest *PBT* at 6.9 years, followed by the ST system at 16.5 years, and finally, the PVT-based system at 21 years.

From an economic standpoint, it is evident that the PVT-based system lacks attractiveness but presents promise for further enhancement. The primary driver impacting economic performance is the investment cost associated with the collectors. PV panels are the most economical

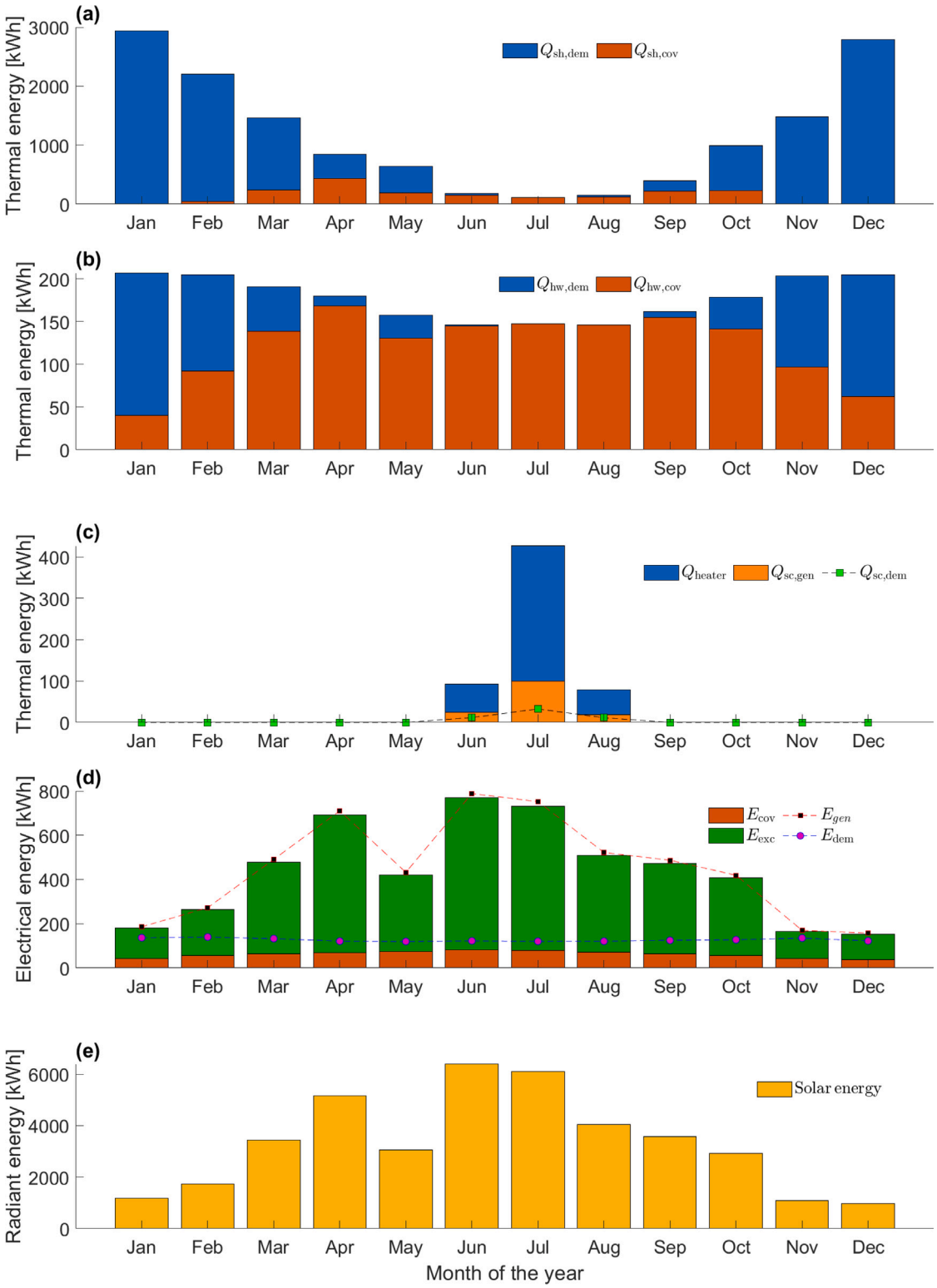

Fig. 6. Total monthly energy in Berlin for (a) Space heating demand ($Q_{sh,dem}$) and covered space heating demand ($Q_{sh,cov}$); (b) hot water demand ($Q_{hw,dem}$) and covered hot water demand ($Q_{hw,cov}$); (c) space cooling demand ($Q_{sc,dem}$), auxiliary heater energy input (Q_{heater}) and DAR generator minimum energy requirements ($Q_{sc,gen}$); (d) electricity demand (E_{dem}), covered electricity (E_{cov}), generated electricity (E_{gen}) and excess electricity (E_{exc}); (e) solar energy. The non-covered demand is met by the auxiliary natural gas heaters and imported electricity.

(€4884), followed by ST collectors (€7470), with PVT collectors being the most expensive (€14,377). Addressing this cost disparity presents a potential avenue for future research and improvement. Furthermore, conducting an economic sensitivity analysis for different key parameters will be further explored in the future, as this is expected to significantly influence the obtained economic results.

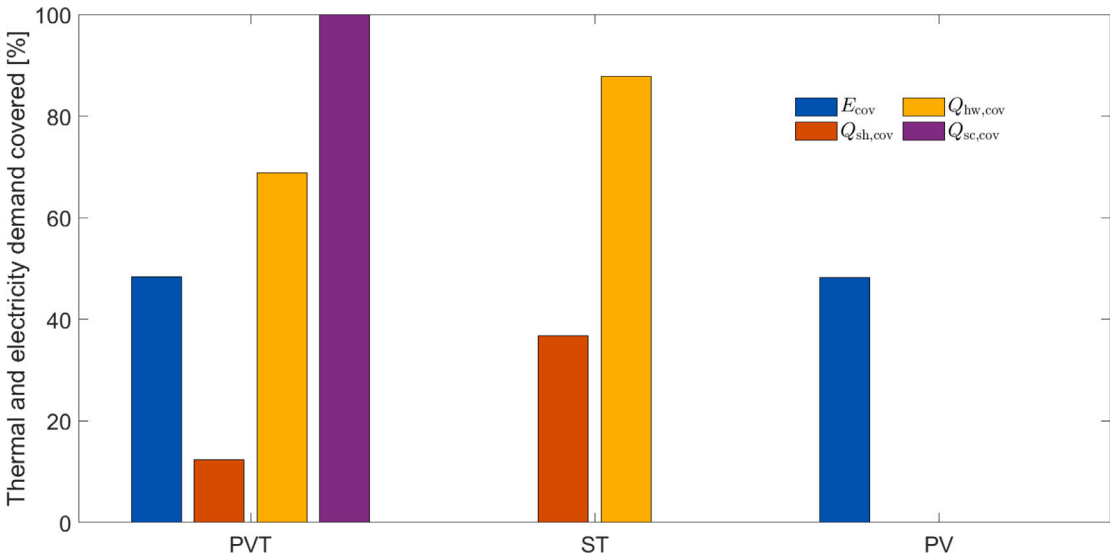

Fig. 7. Comparison of covered demand for electricity (E_{cov}), space heating ($Q_{sh,cov}$), hot water ($Q_{hw,cov}$) and space cooling ($Q_{sc,cov}$) with systems based on PVT, ST and PV, without batteries. The non-covered demand is met by the auxiliary natural gas heaters and imported electricity.

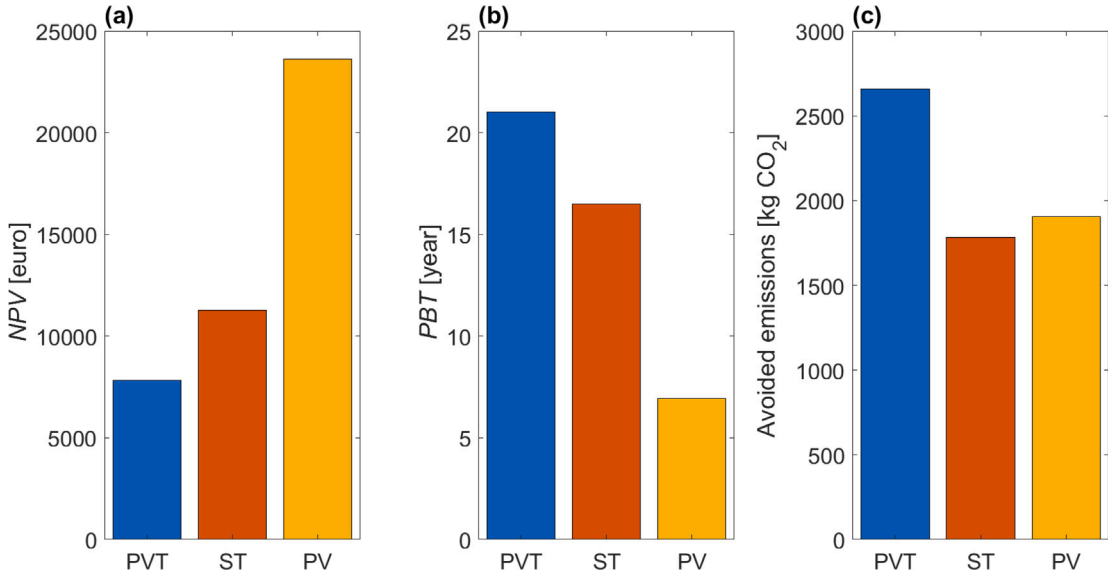

Fig. 8. Comparison of economic and environmental performance for systems based on PVT, ST, and PV: (a) Net present value (*NPV*), (b) payback time (*PBT*) and (c) avoided CO_2-eq emissions.

In terms of environmental performance, PVT collectors demonstrate the most promising outcomes, surpassing both PV and ST systems. PVT collectors demonstrate the highest reduction, with 2658 kg/year of CO_2-eq avoided, followed by the PV system at 1904 kg/year and the ST system at 1781 kg/year, respectively. Despite covering SH and HW demands at slightly lower percentages compared to the ST-based system, PVT collectors offer a distinct advantage: they address all four demands typically encountered in residential settings. This comprehensive coverage reduces dependence on external energy sources, thereby enhancing the energy autonomy of the residential building. Additionally, it reduces electricity consumption for appliances and SC, consequently diminishing dependence on the electric grid, which, in Germany, carries an associated emissions factor of 0.38 kg CO_2-eq/kWh.

3.5. Effect of battery usage

As previously mentioned, the proposed PVT-based system is assumed to operate without battery storage. To evaluate the impact of electricity self-consumption on overall system performance, a sensitivity analysis is conducted, as illustrated in Fig. 9. This analysis explores scenarios in which varying percentages of the household's electricity demand for appliances and lighting, ranging from 0% to 100%, are met directly by electricity generated on-site, with the remaining demand covered by imported grid electricity. The analysis also accounts for the additional investment required to incorporate a typical residential battery, and considers variations in electricity purchase prices and feed-in tariffs across the different scenarios. It is important to highlight that achieving 100% annual self-consumption, where all electricity demand is supplied by on-site generation, is not technically feasible with currently available residential battery technologies. Reaching such levels would require seasonal energy storage (e.g., storing surplus electricity generated in summer for use in winter), which is beyond the capabilities of conventional batteries designed for short-term, daily cycling. As such, the 100% case serves as a theoretical upper bound to illustrate the maximum potential benefit of increased self-consumption, even though it does not reflect realistic operational conditions.

In Fig. 9(a), it is evident that at higher costs of electricity from the grid, while maintaining the selling price of electricity fixed at

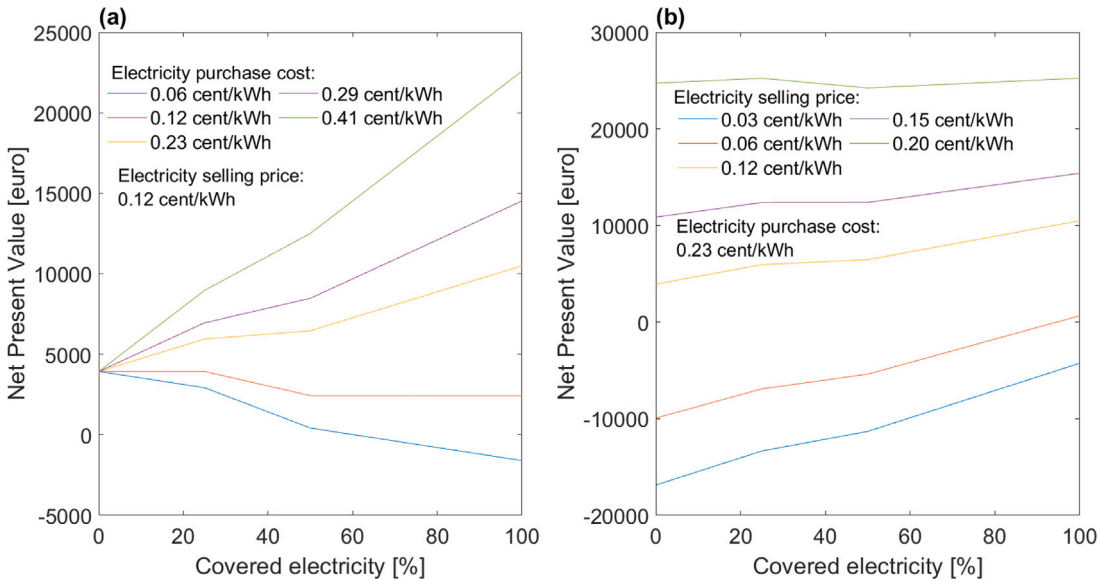

Fig. 9. Net present value as a function of the percentage of electricity demand covered by self-generation with battery storage, and sensitivity to the (a) cost of electricity, at fixed selling price of electricity of 0.12 cent/kWh, and the (b) selling price of electricity to the grid, at fixed cost of electricity from the grid of 0.23 cent/kWh.

0.12 cent/kWh, the option of incorporating batteries to satisfy demand without purchasing power externally becomes more favourable. Notably, at very low prices of electricity, a higher coverage ratio could lead to decreased economic performance, attributed to the opportunity cost of forgoing the sale of excess electricity at 0.12 cent/kWh. In Fig. 9(b), when varying the selling price of electricity while keeping the cost of electricity from the grid fixed at 0.23 cent/kWh, the trends differ from those observed for the cost of electricity. Regardless of the selling price, increasing the coverage ratio in all cases results in a significant improvement in *NPV*. However, it is worth noting that at low selling prices (0.03 and 0.06 cent/kWh), regardless of the coverage ratio with batteries, it would lead to a negative *NPV* for both scenarios. This phenomenon is once again attributed to the opportunity cost associated with not covering internal demand when the cost of electricity exceeds the selling price.

3.6. Analysis and implications

The evolving energy landscape in residential areas demands a fresh perspective on innovative technologies and approaches that not only demonstrate technical reliability but also economic viability and environmental sustainability. Extensive research has underscored the promise of solar energy utilisation, prompting a more thorough examination of its practical applications. This study aimed to evaluate the techno-economic feasibility of a solar-powered system that integrates PVT and DAR technologies. The model was developed under the assumption that PVT collectors cover 40% of the rooftop area, a value calculated in this study as the average of rooftop utilisation factors reported in multiple sources [86–96], applied to an average single-family dwelling in Germany with a roof area of 83 m^2 as indicated in Section 2.4.2. Although these assumptions limit direct extrapolation from the preceding findings of this study, they provide invaluable insights into the technical feasibility, economic viability, and environmental impact of integrating PVT collectors with a DAR system.

Additionally, the study underscores the significance of exploring an organic refrigerant-absorbent combination of *n*-butane/*n*-octane, offering promising avenues for future research in sustainable cooling technologies. The use of alkane mixtures in refrigeration systems offers several advantages over conventional refrigerant-absorbent combinations, such as NH_3-H_2O. Despite their flammability, alkane hydrocarbons demonstrate favourable refrigerant properties and have low environmental impact, potentially reducing risks associated with ozone depletion or global warming. Furthermore, their compatibility with various absorbents, along with their thermal stability, non-toxicity, non-corrosive properties, and enhanced energy efficiency, positions them as promising alternatives that could foster energy savings and minimise environmental impact compared to compression-based systems, closely aligning with the objectives of energy transition initiatives [112,113].

The transient results highlight the critical role of the water tank temperature in determining the energy coverage ratios. This temperature is directly linked to the conditions set in the model, particularly the minimum required temperatures for space heating and hot water demand, as presented in Eq. (6). Throughout a typical winter week, the water tank temperature seldom exceeds 25 °C, which is below the minimum temperatures required for hot water (45 °C) and space heating (60 °C), and as a result, the PVT system alone cannot fully meet these thermal demands. However, it is important to note that the thermal demand not met by the PVT collectors is supplemented by the auxiliary natural gas heater, as illustrated in Fig. 1. Additionally, the transient analysis reveals minimal fluctuation in the water tank temperature despite significant variations in received radiation, underscoring the vital role of the water storage tank in stabilising temperatures and facilitating thermal energy storage.

During a typical summer week, the thermally-driven refrigeration energy requirements are directly examined, assuming full coverage of the total space cooling demand in the model. As the minimum required temperature for the DAR units' generator is consistently unmet, typically ranging between 115–125 °C, and the difference with the water tank temperature exceeds 30–40 °C, it imposes a high thermal energy input from the auxiliary heater providing energy to further increase the hot water coming from the water tank up to the generator's minimum temperature. This is evident in the substantial disparity between the space cooling demand and the actual thermal energy provided by the auxiliary heater, which exceeds the demand by more than 20 times. Recovering used hot water from the DAR units presents a promising area for further research, as this approach could significantly reduce the energy input required from the auxiliary heater for the space cooling system. When comparing the typical weekly profiles, a notable disparity in received irradiance between winter and summer becomes apparent. During summer, irradiance levels peak at around 2000 W/m^2, whereas in winter, they reach a maximum of 700 W/m^2. Additionally, sunlight hours are significantly longer during the summer months. These differences strongly influence the water tank temperature, with temperatures

hovering around 25 °C in winter but soaring to approximately 85 °C in summer. This variance is also reflected in electricity generation, as generation profiles closely track irradiance patterns, resulting in higher generation levels during the summer season.

The monthly and annual results mirror the patterns observed during typical winter and summer weeks. During colder months, only partial hot water and almost no space heating needs are met, with 68% coverage for hot water and only 12% for space heating throughout the year. Additionally, electricity is covered at 48% due to the lack of batteries assumed in the model. While space cooling demand is fully covered, the high thermal energy requirements for the DAR units remain a significant area for further research and improvement. There is still potential for improvement in heat recovery measures and reducing investment costs in collectors to enhance the *NPV*, currently at €7836, and decrease the payback period from the current 21 years to, at least, below 10 years. The analysis of battery presence in the system, along with the sensitivity analysis conducted on electricity selling and cost, represents crucial avenues for further research. It is observed that the economic performance is not inherently improved by the presence of batteries. Rather, it depends on the relative difference between the cost of electricity and selling price of electricity. This highlights the need for more in-depth investigation to understand the impact of battery integration on economic performance and to explore strategies for optimisation in relation to electricity pricing dynamics.

This study opens promising avenues for future research on the PVT-DAR system. A key limitation identified is the temperature difference between the PVT outlet, and consequently the tank water temperature, and the minimum generator temperature required by the DAR unit. Future work could investigate alternative refrigerant–absorbent pairs to identify combinations that lower the generator's minimum operating temperature, as also indicated in [30]. This also underscores the need to develop novel refrigerant-absorbent formulations to improve DAR efficiency by more effectively utilising the thermal output of the PVT collectors. Additionally, recovering hot water from the DAR unit itself could further enhance the overall system efficiency. In parallel, advanced solar collector technologies, such as spectral-splitting and concentrating PVT systems [19], or advanced PVT thermal storage management concepts based on phase change materials, which absorb excess heat to regulate PV cell temperature while enabling subsequent thermal energy utilisation [29], offer a promising pathway to increase outlet temperatures without compromising electricity generation or accelerating PV cell degradation. However, since these technologies currently have a TRL of 3 to 4, corresponding to laboratory and pilot-scale testing [12], their integration into the proposed DAR configuration is not yet considered. Additional research options include also the development of a more detailed model for battery integration, a comprehensive sensitivity analysis of key economic parameters, and the extension of the system analysis to regions with different energy demand profiles, such as Spain, where solar cooling demand is considerably higher. It is important to note that this initial assessment focused on a region with relatively low SC demand to evaluate the DAR system's performance under conditions of limited thermal energy availability. Since the thermal input required by absorption refrigeration systems scales proportionally with cooling demand, using a low-demand context provides a useful baseline for assessing system viability. Finally, future work could also consider strategies for long-term electricity storage, such as storing surplus solar energy generated in summer for use during winter months, which remains a critical challenge for fully autonomous solar-driven systems.

4. Limitations

As previously mentioned, this study provides valuable insights into the feasibility of integrating PVT collectors with a DAR system, yet it is subject to several limitations related to the system configuration and modelling approach. Notably, the system has not been experimentally validated, hot water recovery from the DAR units is not considered, and alternative refrigerant–absorbent pairs have not been comparatively evaluated, which makes the results specific to the chosen fluid combination. Moreover, the model assumes that PVT collectors cover 40% of the 83 m^2 rooftop area of a single-family dwelling in Germany, limiting the applicability of results to other building types, rooftop layouts, or geographic regions. Only commercially available water-based PVT collectors are analysed, making the results specific to this type of collector and excluding advanced technologies such as spectral-splitting PVT. Additionally, while battery integration is evaluated from a high-level perspective, a transient analysis is not considered, constraining the assessment of daily electricity management, and high-level residential energy demand profiles are employed without accounting for occupancy variability or behavioural differences. The economic model has not undergone comprehensive sensitivity analysis despite the significant influence of electricity costs, selling prices, and other parameters on NPV and payback period.

5. Conclusions

This study employed a MATLAB-based model to conduct a comprehensive analysis of the techno-economic and environmental potential of residential solar energy systems, focusing on empirical data. The investigation evaluated the performance and viability of a PVT-based system, compared it with PV and ST systems, and explored the potential integration of battery storage. Key findings and implications are summarised below:

- The achieved energy coverage ratios with the PVT system surpassed those of PV and ST systems, supplying 68% of domestic hot water needs, 48% of electricity demand for appliances and lighting, and 12% of space heating, the latter limited by relatively low temperatures.
- The DAR system successfully met the entire summer cooling demand; however, it required significant auxiliary thermal input due to the limited temperature output from the PVT collectors. This highlights a critical area for improvement in system design and heat recovery, aiming to reduce reliance on auxiliary heating and enhance overall system performance.
- From an economic perspective, the PV system yielded the highest net present value (€23,600), followed by the ST (€11,300) and PVT (€7800) systems, with corresponding payback times of 6.9, 16.5, and 21 years. These results highlight the PV system as the most economically advantageous in terms of long-term financial return.
- In terms of environmental impact, the PVT system proved most effective, avoiding 2658 kg of CO_2-eq emissions annually, compared to 1904 kg/year for PV and 1781 kg/year for ST. This underscores the potential of PVT systems to reduce greenhouse gas emissions and enhance sustainability.
- The integration of batteries increased electricity coverage but did not necessarily improve economic performance, as outcomes are highly dependent on the regional economic context.
- Overall, the findings emphasise the importance of balancing economic viability and environmental sustainability when designing and deploying residential renewable energy systems.

CRediT authorship contribution statement

Jeremias E. Castro: Writing – original draft, Validation, Software, Investigation. **Andreas V. Olympios:** Writing – review & editing, Software, Resources. **Asmaa A. Harraz:** Writing – review & editing, Validation, Software, Resources. **Bryce S. Richards:** Writing – review & editing, Formal analysis, Data curation. **Jingyuan Xu:** Writing – review & editing, Resources, Project administration, Methodology, Funding acquisition, Conceptualization, Supervision.

Declaration of competing interest

The authors declare that they have no known competing financial interests or personal relationships that could have appeared to influence the work reported in this paper.

Appendix A. Pumping power calculation

The electrical power required by the pump circulating the heat transfer fluid in the PVT and ST systems is estimated from:

$$\dot{W}_{\text{pump,collectors}} = \frac{\dot{m}_{\text{fa}} \left(\Delta P_{\text{collectors}} + \Delta P_{\text{system,collectors}} \right)}{\eta_{\text{pump}}\, \rho}, \tag{A.1}$$

where $\dot{W}_{\text{pump,collectors}}$ is the pump power consumption in watts, $\dot{m}_{\text{fa}}$ the total mass flow rate through the collectors in kg/s (70 L/h per PVT collector and 120 L/h per ST collector), $\Delta P_{\text{collectors}}$ the pressure drop across the collectors in Pa, $\Delta P_{\text{system,collectors}}$ the pressure drop in the loop system in Pa, η_{pump} the pump efficiency (assumed 85%), and ρ the density of the heat transfer fluid (water) in $\text{kg}\,\text{m}^{-3}$. The pressure drop in the PVT and ST loop systems is calculated as:

$$\Delta P_{\text{system,collectors}} = \left(\frac{f L}{D_{\text{h}}} \right) 0.5\, \rho \left(\frac{\dot{m}_{\text{fa}}}{\rho A} \right)^2, \tag{A.2}$$

where f is the Darcy–Weisbach friction factor [114], L the total pipe length (m), D_{h} the hydraulic diameter (m), and A the internal cross-sectional area of the pipes (m^2). The pressure drop across each collector is taken as constant at $0.18 \cdot 10^5$ Pa, based on averaged literature values [115,116].

The pump power for circulating water in the cooling system is calculated analogously:

$$\dot{W}_{\text{pump,cooling}} = \frac{\dot{m}_{\text{sc,cov}} \Delta P_{\text{system,cooling}}}{\eta_{\text{pump}}\, \rho}, \tag{A.3}$$

where $\dot{m}_{\text{sc,cov}}$ is the cooling-loop mass flow rate ($0.25\ \text{kg}\,\text{s}^{-1}$). The cooling-loop system pressure drop is obtained as:

$$\Delta P_{\text{system,cooling}} = \left(\frac{f L}{D_{\text{h}}} \right) 0.5\, \rho \left(\frac{\dot{m}_{\text{sc,cov}}}{\rho A} \right)^2, \tag{A.4}$$

with parameters f, L, D_{h}, and A defined as above but for the cooling system.

Appendix B. Heat transfer correlations for coil and tank

The heat transfer from the fluid inside the coil-type heat exchanger to the water tank is modelled using the following equations. The effectiveness ε is determined as a function of the number of transfer units (NTU) employing the correlation:

$$\varepsilon = 1 - e^{(-NTU)} \tag{B.1}$$

The NTU is calculated as:

$$NTU = \frac{1}{R_{\text{coil}} c_{\text{p,water}} \dot{m}_{\text{fa}}} \tag{B.2}$$

The thermal resistance, denoted as R_{coil}, takes into account forced convection in the coil, natural convection in the tank, and the thermal resistance of the pipe walls, and is calculated as:

$$R_{\text{coil}} = \frac{D_{\text{o}}}{D_{\text{i}} h_{\text{coil}}} + D_{\text{o}} \frac{\ln\left(\frac{D_{\text{o}}}{D_{\text{i}}} \right)}{2 k_{\text{p}}} + \frac{1}{h_{\text{wt}}} \tag{B.3}$$

Here, k_{p} represents the thermal conductivity of the copper pipe of the coil, while D_{i} and D_{o} stand for the internal and outside diameter of the coil, respectively.

The forced convection within the coil-type heat exchanger, h_{coil}, as derived from [117,118], is expressed as follows:

$$h_{\text{coil}} = \frac{\text{Nu}_{\text{coil}} k_{\text{fluid}}}{D_{\text{i}}}, \tag{B.4}$$

where k_{fluid} is the thermal conductivity of water, and Nu_{coil} represents the Nusselt number for the water circulating through the coil, defined by:

$$\text{Nu}_{\text{coil}} = \begin{cases} 3.66 + 0.08 \left[1 + 0.8 \left(\frac{D_{\text{i}}}{D_{\text{o}}} \right)^{0.9} \right] (\text{Re}_{\text{coil}})^m \text{Pr}^{0.3}, & \text{if } \text{Re}_{\text{coil}} < \text{Re}_{\text{critic}} \\ 0.023 (\text{Re}_{\text{coil}})^{0.85} \text{Pr}^{0.4}, & \text{if } \text{Re}_{\text{coil}} \geq \text{Re}_{\text{critic}} \end{cases} \tag{B.5}$$

Here, Pr is the Prandtl number ($\mu c_{p,\text{water}} / k_{\text{fluid}}$), and $\text{Re}_{\text{critic}}$ is the critical Reynolds number given by:

$$\text{Re}_{\text{critic}} = 2300 \left[1 + 8.6 \left(\frac{D_{\text{i}}}{D_{\text{o}}} \right)^{0.45} \right], \tag{B.6}$$

and, Re_{coil} is the Reynolds number for the water circulating in the coil, calculated as:

$$\text{Re}_{\text{coil}} = \frac{4 \dot{m}_{\text{fa}}}{\pi D_{\text{i}} \mu} \tag{B.7}$$

While the coefficient m is defined as:

$$m = 0.5 + 0.29 \left(\frac{D_{\text{i}}}{D_{\text{o}}} \right)^{0.19} \tag{B.8}$$

The laminar natural convection heat transfer coefficient inside the water tank is modelled using an experimentally determined equation from [119]:

$$h_{\text{wt}} = \frac{\text{Nu}_{\text{tank}} k_{\text{fluid}}}{D_{\text{o}}}, \tag{B.9}$$

where the Nusselt number is computed based on the Rayleigh number as follows:

$$\text{Nu}_{\text{tank}} = 0.52 \left(\text{Ra}_{\text{tank}} \right)^{0.25} \tag{B.10}$$

Appendix C. DAR model error analysis

Eqs. (8) and (9) of the DAR model require experimentally derived coefficients, which originate from the experimental work documented in [38] and were provided by the author for use in the present study. Additional details on the DAR thermodynamic model are available in a

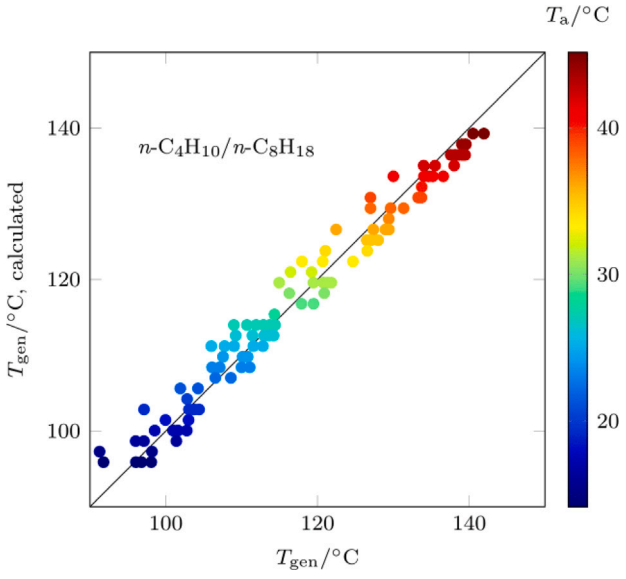

Fig. C.1. Comparison of measured and calculated generator temperatures (T_{gen} and $T_{\text{gen,calculated}}$) using the DAR model at various ambient temperatures (T_{amb}) with the nC$_4$-nC$_8$ refrigerant–absorbent combination.

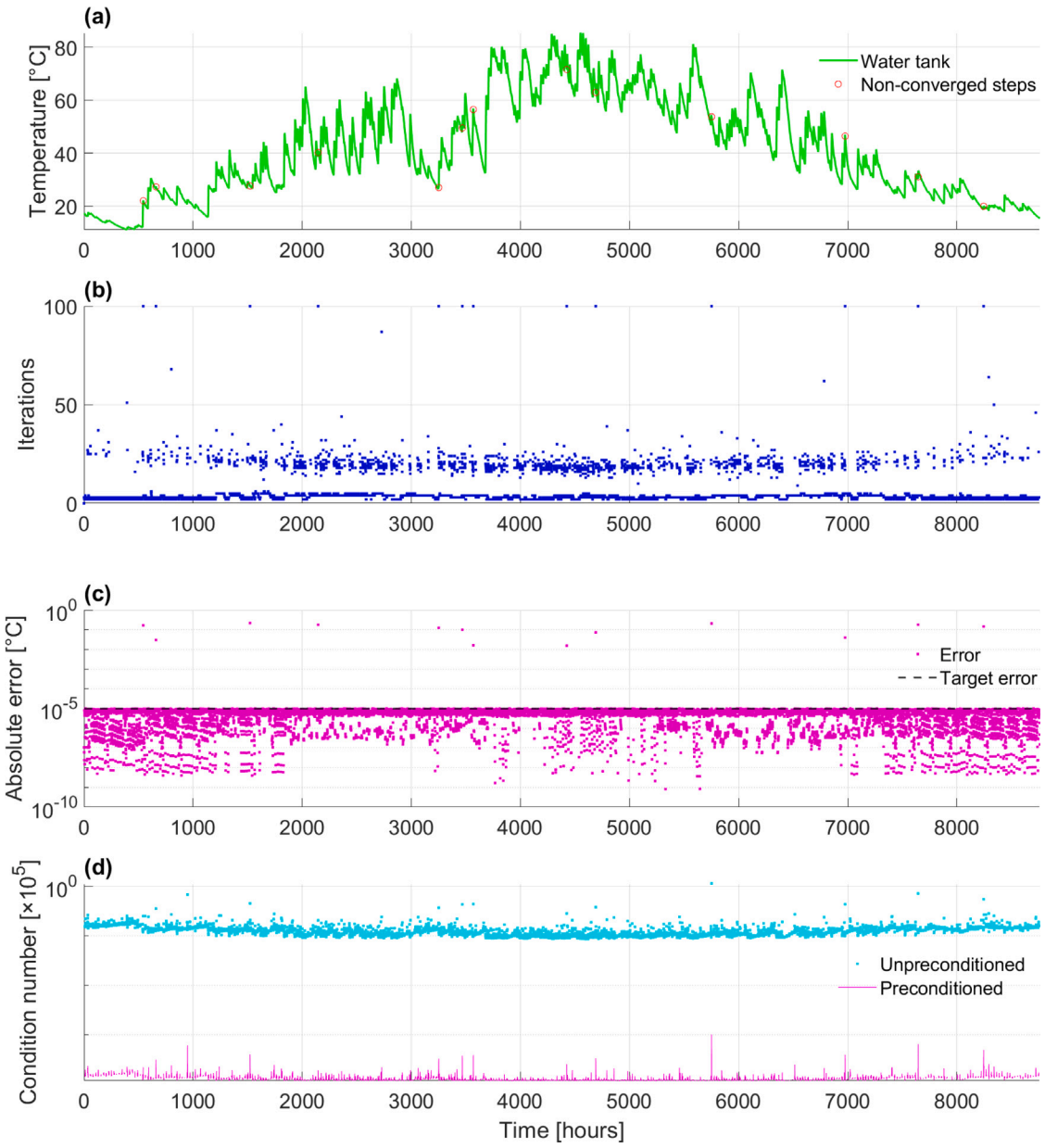

Fig. D.1. Convergence analysis of the numerical solution over 8760 hourly time steps: (a) Water tank temperature (T_{wt}) profile, with non-converged steps shown in red; (b) Iterations to convergence per time step (maximum of 100); (c) Absolute error at convergence, with the target threshold indicated by a dashed line; (d) Condition number of the Backward Euler system matrix before and after diagonal preconditioning.

recent study by the same research group [57]. Model–experiment deviations are quantified using the Percentage Average Absolute Deviation ($\%AAD$), defined as:

$$\%AAD = \left[\frac{1}{N}\sum_{i=1}^{N}\frac{|X_i^{\exp} - X_i^{\text{calc}}|}{\bar{X}^{\exp}}\right] \times 100 \tag{C.1}$$

where $X_i^{\exp}$ and X_i^{calc} denote the ith experimental and calculated values, respectively; N is the number of data points; and $\bar{X}^{\exp}$ is the mean experimental measurement.

For illustration purposes, Fig. C.1 shows the measured and predicted generator wall temperatures (T_{gen} and $T_{\text{gen,calculated}}$) across varying ambient temperatures (T_{amb}) for the $n\text{C}_4$-$n\text{C}_8$ working combination. For this pair, the model yields a $\%AAD$ of 0.53% for the generator wall temperature (Eq. (8)) and 30% for the cooling rate prediction (Eq. (9)). These results indicate that the DAR model provides excellent agreement with experimental measurements for the generator wall temperature, as evidenced by the very low %AAD. The higher %AAD observed for the cooling rate reflects limitations in capturing dynamic thermal interactions within the simplified model; however, this level of deviation is considered acceptable for the purposes of system-level performance analysis.

Appendix D. Model numerical validation

The numerical validation assesses the convergence, stability, and accuracy of the solution method applied to the mathematical model presented in Section 2.2. The model employs an iterative scheme to address the non-linearity of the coupled equations governing the PVT energy balance (Eq. (2)), the water tank energy balance (Eq. (4)), and the coil-type heat exchanger (Eq. (5)). This non-linearity primarily arises from the empirical correlation used to determine the coil heat transfer coefficient, as discussed in Appendix B. The solution procedure is structured in two stages. For each hourly time step, a fixed-point iteration is applied to resolve the system's non-linearities. Within each

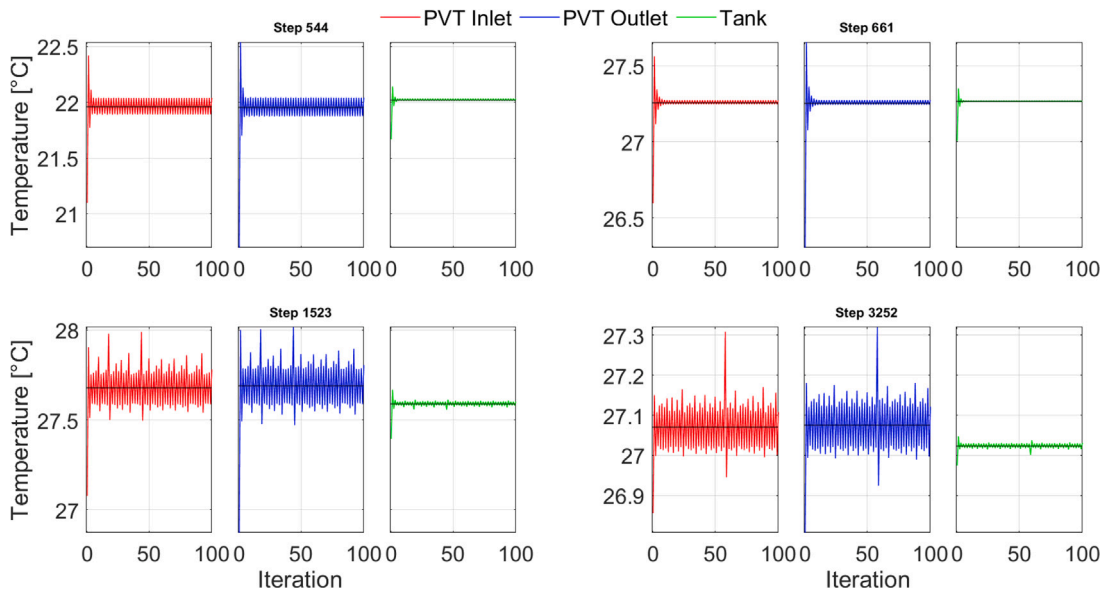

Fig. D.2. Iteration histories of four representative non-converged steps showing bounded oscillatory behaviour. Each step has three subplots for $T_{\mathrm{PVT,inlet}}$, $T_{\mathrm{PVT,outlet}}$, and T_{wt}. Steps 544 and 661 represent typical non-converged points, showing smaller, stable oscillations, whereas steps 1523 and 3252 correspond to extreme cases with larger oscillations. Black dashed lines indicate the mean temperatures.

iteration, the coupled equations are discretised in time using the implicit Backward Euler scheme and solved accordingly. The validation therefore examines both the iterative non-linear solver and the implicit time-stepping method.

Fig. D.1 summarises the full-year convergence analysis. Subplot (a) shows the water tank temperature over the year, highlighting non-converged steps. These points are scattered rather than clustered, indicating that non-convergence is unrelated to specific operating conditions and instead corresponds to isolated instances exceeding the prescribed error tolerance and maximum iterations. The iteration counts are shown in subplot (b) for converged steps: average of 5.74, 90th percentile of 18, and 99th percentile of 26. Subplot (c) presents the absolute error for converged steps, with an average of $2.71 \cdot 10^{-6}$ °C, 90th percentile of $7.70 \cdot 10^{-6}$ °C, and 99th percentile of $9.72 \cdot 10^{-6}$ °C, well below the $1 \cdot 10^{-5}$ °C tolerance after 100 iterations. To assess the impact of preconditioning on the numerical stability and convergence of the implicit method, a diagonal preconditioner was implemented from the diagonal elements of the system matrix to reduce its condition number, as indicated in [120,121]. Subplot (d) compares the condition numbers before and after preconditioning, showing a marked reduction. Nevertheless, the simulation results remained essentially unchanged, indicating that the attainable accuracy and convergence rate are constrained by the fixed-point iteration rather than by the Backward Euler scheme.

Further analysis examines four representative steps from the 13 out of 8760 (approximately 0.15%) that do not meet the convergence criterion within 100 iterations (Fig. D.2). The iteration histories for $T_{\mathrm{PVT,in}}$, $T_{\mathrm{PVT,out}}$, and T_{wt} reveal bounded, low-amplitude oscillations around the solution rather than divergence. In all cases, the error remains on the order of $1 \cdot 10^{-1}$ °C, which is acceptable for this system-level, hourly-resolution simulation and has no noticeable impact on the annual performance results. Steps 544 and 661 typify most non-converged points, showing relatively small and stable oscillation bounds. The two more extreme cases, steps 1523 and 3252, exhibit wider oscillation margins, yet the absolute error still remains around $1 \cdot 10^{-1}$ °C.

In summary, the Backward Euler method demonstrated robust performance, while the fixed-point iteration introduced only a small number of non-converged steps that still remained within acceptable bounds. Although a more advanced solver (e.g., Newton–Raphson) could potentially eliminate these isolated cases, the chosen fixed-point approach provides an effective balance between accuracy, stability, and computational efficiency for the model's intended application.

Data availability

Data will be made available on request.

References

[1] Lee H, Romero J. Summary for policymakers. In: Climate change 2023: Synthesis report. contribution of working groups I, II and III to the sixth assessment report of the intergovernmental panel on climate change. Tech. rep., Intergovernmental Panel on Climate Change; 2023, p. 1–34. http://dx.doi.org/10.59327/IPCC/AR6-9789291691647.001.

[2] Fernández A, Spencer T, et al. Net zero roadmap: A global pathway to keep the 1.5 ° C goal in reach, International Energy Agency, Paris. International Energy Agency; 2023, https://iea.blob.core.windows.net/assets/9a698da4-4002-4e53-8ef3-31d8971bf84/NetZeroRoadmap_AGlobalPathwaytoKeepthe1.5CGoalinReach-2023Update.pdf. [Accessed: April 2024].

[3] World Economic Forum, https://www.weforum.org/communities/gfc-on-energy-transition/ (2023).

[4] IEA. Global energy review 2025. Tech. rep, International Energy Agency; 2025, https://www.iea.org/reports/global-energy-review-2025/.

[5] Global CO2 emissions from the operation of buildings in the Net zero scenario, 2010–2030. International Energy Agency; 2023, https://www.iea.org/data-and-statistics/charts/global-co2-emissions-from-the-operation-of-buildings-in-the-net-zero-scenario-2010-2030. [Accessed: April 2024].

[6] Christopher S, Vikram M, Bakli C, Thakur AK, Ma Y, Ma Z, Xu H, Cuce PM, Cuce E, Singh P. Renewable energy potential towards attainment of net-zero energy buildings status – a critical review. J Clean Prod 2023;405:136942. http://dx.doi.org/10.1016/j.jclepro.2023.136942.

[7] Gul E, Baldinelli G, Bartocci P, Shamim T, Domenighini P, Cotana F, Wang J, Fantozzi F, Bianchi F. Transition toward net zero emissions - integration and optimization of renewable energy sources: Solar, hydro, and biomass with the local grid station in central Italy. Renew Energy 2023;207:672–86. http://dx.doi.org/10.1016/j.renene.2023.03.051.

[8] Noh Y, Jafarinejad S, Anand P. A review on harnessing renewable energy synergies for achieving urban net-zero energy buildings: Technologies, performance evaluation, policies, challenges, and future direction. Sustainability 2024;16(8). http://dx.doi.org/10.3390/su16083444.

[9] Hachem-Vermette C. Role of solar energy in achieving net zero energy neighborhoods. Sol Energy Adv 2022;2:100018. http://dx.doi.org/10.1016/j.seja.2022.100018.

[10] Maduta C, Melica G, D'Agostino D, Bertoldi P. Towards a decarbonised building stock by 2050: The meaning and the role of zero emission buildings (ZEBs) in europe. Energy Strat Rev 2022;44:101009. http://dx.doi.org/10.1016/j.esr.2022.101009.

[11] Noh Y, Jafarinejad S, Anand P. A review on harnessing renewable energy synergies for achieving urban net-zero energy buildings: Technologies, performance evaluation, policies, challenges, and future direction. Sustainability 2024;16(8). http://dx.doi.org/10.3390/su16083444.

[12] Herrando M, Wang K, Huang G, Otanicar T, Mousa OB, Agathokleous RA, Ding Y, Kalogirou S, Ekins-Daukes N, Taylor RA, Markides CN. A review of solar hybrid photovoltaic-thermal (PV-t) collectors and systems. Prog Energy Combust Sci 2023;97:101072. http://dx.doi.org/10.1016/j.pecs.2023.101072.

[13] Xu J, Song J, Huang G, Mersch M, Wang K, Markides CN. Comprehensive comparative assessments of optimal distributed solar-energy systems for combined heat and power. Energy 2026;344:139724. http://dx.doi.org/10.1016/j.energy.2025.139724.

[14] Aslam A, Ahmed N, Qureshi SA, Assadi M, Ahmed N. Advances in solar PV systems; a comprehensive review of PV performance, influencing factors, and mitigation techniques. Energies 2022;15(20). http://dx.doi.org/10.3390/en15207595.

[15] Han H, Kurses M, Harraz AA, Xu J. Comparative study of PV, PVT, and solar thermal systems for residential applications in Europe. Energy 2025;336:138368. http://dx.doi.org/10.1016/j.energy.2025.138368.

[16] Ghazy M, Ibrahim E, Mohamed A, et al. Cooling technologies for enhancing photovoltaic–thermal (PVT) performance: a state of the art. Int J Energy Env Eng 2022;13:1205–35. http://dx.doi.org/10.1007/s40095-022-00491-8.

[17] Pathak SK, Sharma PO, Goel V, Bhattacharyya S, Aybar H, Meyer JP. A detailed review on the performance of photovoltaic/thermal system using various cooling methods. Sustain Energy Technol Assessments 2022;51:101844. http://dx.doi.org/10.1016/j.seta.2021.101844.

[18] Madurai Elavarasan R, Mudgal V, Selvamanohar L, Wang K, Huang G, Shafiullah G, Markides CN, Reddy K, Nadarajah M. Pathways toward high-efficiency solar photovoltaic thermal management for electrical, thermal and combined generation applications: A critical review. Energy Convers Manage 2022;255:115278. http://dx.doi.org/10.1016/j.enconman.2022.115278.

[19] Ghaith F, Siddiqui T, Nour M. Design of solar-powered cooling systems using concentrating photovoltaic/thermal systems for residential applications. Energies 2024;17(18). http://dx.doi.org/10.3390/en17184558.

[20] Zenhäusern D, Evelyn B, Aleksis B. PVT wrap-up: Energy systems with photovoltaic-thermal solar collectors. Swiss Federal Office of Energy (SFOE); 2017, https://www.ost.ch/fileadmin/dateiliste/3_forschung_dienstleistung/institute/spf/forschung/publikationen/pvt_wrapup_final_en.pdf. [Accessed: April 2024].

[21] Najjaran A, Harraz A, Freeman J, Dowell NM, Markides C. Numerical and experimental investigation of diffusion absorption refrigeration systems for use with low-temperature heat sources, vol. 31. 31, 2018, http://hdl.handle.net/10044/1/62182.

[22] Mansouri R. Theoretical and experimental study of absorption and absorption/diffusion refrigerating machines using ammonia as a refrigerant: simulation under steady-state and dynamic regimes and experimental characterization of a pilot [Ph.D. thesis], Universitat Rovira i Virgili; 2016, http://hdl.handle.net/10803/399538.

[23] Harraz AA, Freeman J, Wang K, Dowell NM, Markides CN. Diffusion-absorption refrigeration cycle simulations in gPROMS using SAFT mie. Energy Procedia 2019;158:2360–5. http://dx.doi.org/10.1016/j.egypro.2019.01.284, Innovative Solutions for Energy Transitions.

[24] Ramos A, Chatzopoulou MA, Guarracino I, Freeman J, Markides CN. Hybrid photovoltaic-thermal solar systems for combined heating, cooling and power provision in the urban environment. Energy Convers Manage 2017;150:838–50. http://dx.doi.org/10.1016/j.enconman.2017.03.024.

[25] Herrando M, Simón R, Guedea I, Fueyo N. The challenges of solar hybrid PVT systems in the food processing industry. Appl Therm Eng 2021;184:116235. http://dx.doi.org/10.1016/j.applthermaleng.2020.116235.

[26] Monghasemi N, Vouros S, Kyprianidis K, Vadiee A. Performance assessment of a photovoltaic/thermal-powered absorption chiller for a restaurant. In: Proceedings of the 64th international conference of scandinavian simulation society. 2023, http://dx.doi.org/10.3384/ecp200017, https://ecp.ep.liu.se/index.php/sims/article/view/758.

[27] Jiao C, Li Z. An updated review of solar cooling systems driven by photovoltaic–thermal collectors. Energies 2023;16(14). http://dx.doi.org/10.3390/en16145331.

[28] Najafi Roudbari F, Ehsani H, Amiri S, Samadani A, Shabani S, Khodadad A. Advances in photovoltaic thermal systems: A comprehensive review of CPVT and PVT technologies. Sol Energy Mater Sol Cells 2024;276:113070. http://dx.doi.org/10.1016/j.solmat.2024.113070.

[29] Hamada A, Emam M, Refaey H, Moawed M, Abdelrahman M. Investigating the performance of a water-based PVT system using encapsulated PCM balls: An experimental study. Energy 2023;284:128574. http://dx.doi.org/10.1016/j.energy.2023.128574.

[30] Kurses M, Olympios AV, Harraz AA, Xu J. Comparative analysis of heating and cooling solutions for residential use: Energy, environmental, and economic perspectives. Appl Energy 2025;399:126511. http://dx.doi.org/10.1016/j.apenergy.2025.126511.

[31] Kim G, Choi HW, Lee G, Lee JS, Kang YT. Experimental study on diffusion absorption refrigeration systems with low GWP refrigerants. Energy 2020;201:117626. http://dx.doi.org/10.1016/j.energy.2020.117626.

[32] Garma R, Ben-Ezzine N, Bellagi A. Experimental and numerical investigation on diffusion-absorption refrigeration system using low GWP refrigerant R600, C9h20 and helium. Int J Thermofluids 2025;27:101246. http://dx.doi.org/10.1016/j.ijft.2025.101246.

[33] Arnesson H, Olympios AV, Harraz AA, Xu J. Comprehensive energy, economic, and environmental analysis of a hybrid photovoltaic–thermal (PVT) heat pump system. Energy 2025;331:136563. http://dx.doi.org/10.1016/j.energy.2025.136563.

[34] Vallati A, Di Matteo M, Lo Basso G, oń PO, Fiorini CV. Definition of a PVT coupled water source heat pump system through optimization of individual components. Energy 2024;307:132455. http://dx.doi.org/10.1016/j.energy.2024.132455.

[35] Vallati A, Di Matteo M, Sundararajan M, Muzi F, Fiorini CV. Development and optimization of an energy saving strategy for social housing applications by water source-heat pump integrating photovoltaic-thermal panels. Energy 2024;301:131531. http://dx.doi.org/10.1016/j.energy.2024.131531.

[36] Freeman J, Markides C. A solar diffusion-absorption refrigeration system for off-grid cold-chain provision, part II: System simulation and assessment of performance. Renew Energy 2024;230:120717. http://dx.doi.org/10.1016/j.renene.2024.120717.

[37] International Energy Agency, https://www.iea.org/commentaries/staying-cool-without-overheating-the-energy-system. [accessed: December 2025].

[38] Harraz A. Computer-aided molecular and system design of diffusion absorption solar-cooling systems [Ph.D. thesis], Imperial College of Science, Technology and Medicine. Department of Chemical Engineering; 2022.

[39] Bauer T, Steinmann W-D, Laing D, Tamme R. Thermal energy storage materials and systems. Annu Rev Heat Transf 2012;15:131–77. http://dx.doi.org/10.1615/AnnualRevHeatTransfer.2012004651.

[40] Herrando M, Pantaleo AM, Wang K, Markides CN. Solar combined cooling, heating and power systems based on hybrid PVT, PV or solar-thermal collectors for building applications. Renew Energy 2019;143:637–47. http://dx.doi.org/10.1016/j.renene.2019.05.004.

[41] Wang K, Herrando M, Pantaleo AM, Markides CN. Technoeconomic assessments of hybrid photovoltaic-thermal vs. conventional solar-energy systems: Case studies in heat and power provision to sports centres. Appl Energy 2019;254:113657. http://dx.doi.org/10.1016/j.apenergy.2019.113657.

[42] Hosouli S, Gomes J, Loris A, Pazmiño I-A, Naidoo A, Lennermo G, Mohammadi H. Evaluation of a solar photovoltaic thermal (PVT) system in a dairy farm in Germany. Sol Energy Adv 2023;3:100035. http://dx.doi.org/10.1016/j.seja.2023.100035.

[43] Herrando M, Ramos A, Freeman J, Zabalza I, Markides CN. Technoeconomic modelling and optimisation of solar combined heat and power systems based on flat-box PVT collectors for domestic applications. Energy Convers Manage 2018;175:67–85. http://dx.doi.org/10.1016/j.enconman.2018.07.045.

[44] Herrando M, Guarracino I, del Amo A, Zabalza I, Markides CN. Energy characterization and optimization of new heat recovery configurations in hybrid PVT systems. 2016, http://dx.doi.org/10.18086/eurosun.2016.08.22.

[45] Herrando M, Ramos A, Zabalza I, Markides CN. A comprehensive assessment of alternative absorber-exchanger designs for hybrid PVT-water collectors. Appl Energy 2019;235:1583–602. http://dx.doi.org/10.1016/j.apenergy.2018.11.024.

[46] Herrando M, Fantoni G, Cubero A, Simón-Allué R, Guedea I, Fueyo N. Numerical analysis of the fluid flow and heat transfer of a hybrid PV-thermal collector and performance assessment. Renew Energy 2023;209:122–32. http://dx.doi.org/10.1016/j.renene.2023.03.125.

[47] Ecomesh. Endef; 2023, https://endef.com/en/hybrid-solar-panel/ecomesh/. [Accessed: April 2024].

[48] Ecovolt. Endef; 2023, https://endef.com/en/hybrid-solar-panel/ecovolt/. [Accessed: April 2024].

[49] DualSun, https://dualsun.com/wp-content/uploads/dualsun-fr-fiche-technique-spring-280.pdf. [Accessed: April 2024] (2023).

[50] CPVT60P250. Crane; 2023, https://solarphotovoltaic.biz. [Accessed: April 2024].

[51] 300W Ecovolt hybrid solar panel. Todoensolar; 2023, https://www.todoensolar.com/300w-ecovolt-hybrid-solar-panel. [Accessed: April 2024].

[52] Panel solar híbrido 250W / 24V agua caliente y electricidad. Todoensolar; 2023, https://www.todoensolar.com/epages/61987244.sf/es_ES/?bjectPath=/Shops/61987244/Products/pvtcrane. [Accessed: April 2024].

[53] CPVT60P250. Crane; 2023, https://www.crane-bg.com/en. [Accessed: April 2024].

[54] Panel solar hibrido de 265W ecomesh. Todoensolar; 2023, https://www.todoensolar.com/panel-solar-hibrido-265w-ecomesh. [Accessed: April 2024].

[55] Panneau solaire hybride PVT non isolé. myshop-solaire; 2023, https://www.myshop-solaire.com/panneau-solaire-spring-425w-shingle-black-dual-sun-_r_951_i_4560.html. [Accessed: April 2024].

[56] Zhu S, Wang K, González-Pino I, Song J, Yu G, Luo E, Markides CN. Techno-economic analysis of a combined heat and power system integrating hybrid photovoltaic-thermal collectors, a stirling engine and energy storage. Energy Convers Manage 2023;284:116968. http://dx.doi.org/10.1016/j.enconman.2023.116968.

[57] Harraz AA, Haslam AJ, Mac Dowell N, Markides CN. Computer-aided molecular design of diffusion–absorption refrigeration modules for low-temperature solar collectors. Energy Convers Manage 2025;343:120067. http://dx.doi.org/10.1016/j.enconman.2025.120067.

[58] Schmid F, Spindler K. Experimental investigation of the auxiliary gas circuit of a diffusion absorption chiller with natural and forced circulation. Int J Refrig 2016;70:84–92. http://dx.doi.org/10.1016/j.ijrefrig.2016.07.012.

[59] Yıldız A, Ersöz MA. Energy and exergy analyses of the diffusion absorption refrigeration system. Energy 2013;60:407–15. http://dx.doi.org/10.1016/j.energy.2013.07.062.

[60] Kingspan Solar, https://www.thema-sa.be/notices/kingspan/nt_HP400-DF400.pdf. [Accessed: April 2024].

[61] Olympios AV, Mersch M, Sapin P, Pantaleo AM, Markides CN. Library of price and performance data of domestic and commercial technologies for low-carbon energy systems. 2021, http://dx.doi.org/10.5281/zenodo.4692649.

[62] Reise C, Müller B, Heydenreich W. Describing the world with three parameters: A new approach to PV module power modelling. 2008, https://api.semanticscholar.org/CorpusID:107703903. [Accessed: April 2024].

[63] ISO 9806:2017-Solar energy-Solar thermal collectors-Test methods. International Organization for Standardization; 2017, https://www.iso.org/standard/67978.html. [Accessed: April 2024].

[64] Allan J, Dehouche Z, Stankovic S, Mauricette L. Performance testing of thermal and photovoltaic thermal solar collectors. Energy Sci Eng 2015;3(4):310–26. http://dx.doi.org/10.1002/ese3.75.

[65] Duffie J, Beckman W. Solar engineering of thermal processes. John Wiley and Sons; 2013, http://dx.doi.org/10.1002/9781118671603.

[66] What temperature should my combi boiler be set at?. Vaillant; 2023, https://www.vaillant.co.uk/homeowners/advice-and-knowledge/combiboilertemperaturesetting-2156808.html. [Accessed: April 2024].

[67] Otanicar T, Taylor RA, Phelan PE. Prospects for solar cooling – an economic and environmental assessment. Sol Energy 2012;86(5):1287–99. http://dx.doi.org/10.1016/j.solener.2012.01.020.

[68] Kakaç S, Bergles A, Fernandes O. Two-phase flow heat exchangers: Thermal-hydraulic fundamentals and design. In: E:applied sciences, vol. 143, Kluwer Academic Publishers; 1987, http://dx.doi.org/10.1007/978-94-009-2790-2.

[69] Bisulandu M, Robert B-J, Mansouri R, Ilinca A. Diffusion absorption refrigeration systems: An overview of thermal mechanisms and models. Energies 2023;16(9). http://dx.doi.org/10.3390/en16093610.

[70] Villa AAO, Costa JAPd, Santos CACd. Energetic analysis using theoretical modeling and the characteristic equation method in a small absorption chiller with LiBr/H2O. Acta Sci Technol 2018;40(1):e34969. http://dx.doi.org/10.4025/actascitechnol.v40i1.34969.

[71] Kini G, Chandrasekaran S, Tambasco M, Garimella S. A residential absorption chiller for high ambient temperatures. Int J Refrig 2020;120:31–8. http://dx.doi.org/10.1016/j.ijrefrig.2020.08.022.

[72] Taieb A, Mejbri K, Bellagi A. Detailed thermodynamic analysis of a diffusion-absorption refrigeration cycle. Energy 2016;115:418–34. http://dx.doi.org/10.1016/j.energy.2016.09.002.

[73] Freeman J, Najjaran1 A, Edwards R, Reid M, Hall R, Ramos A, Markides CN. Testing and simulation of a solar diffusion-absorption refrigeration system for low-cost solar cooling in India. 2017, http://dx.doi.org/10.18086/swc.2017.28.07.

[74] Turton R, Shaeiwitz J, Bhattacharyya D, Whiting W. Analysis, synthesis and design of chemical processes 5ed.. In: Prentice hall international series in the physical and chemical engineering sciences, Pearson Education; 2018, p. 250–1.

[75] Ueckerdt F, Hirth L, Luderer G, Edenhofer O. System LCOE: What are the costs of variable renewables? Energy 2013;63:61–75. http://dx.doi.org/10.1016/j.energy.2013.10.072.

[76] Mai T, Mowers M, Eurek K. Competitiveness metrics for electricity system technologies. Tech. rep, National Renewable Energy Laboratory; 2021, https://www.nrel.gov/docs/fy21osti/72549.pdf.

[77] Euro-Negoce, https://www.euro-negoce.fr/en/gas-boiler/2925-gas-wall-mounted-boiler-de-dietrich-mcr2-35-bic.html. [Accessed: April 2024].

[78] GreenCentral, https://www.greencentral.co.uk/product/viessmann-vitodens-100-w-30kw-gas-combi-boiler/. [Accessed: April 2024].

[79] GreenCentral, https://www.greencentral.co.uk/product/ideal-heating-vogue-max-32kw-gas-combi-boiler/. [Accessed: April 2024].

[80] Quoilin S, Declaye S, Tchanche BF, Lemort V. Thermo-economic optimization of waste heat recovery organic rankine cycles. Appl Therm Eng 2011;31(14):2885–93. http://dx.doi.org/10.1016/j.applthermaleng.2011.05.014.

[81] Masson G, de l'Epine M, Kaizuka I. Trends in photovoltaic applications 2024. Tech. rep, IEA Photovoltaic Power Systems Programme (IEA-PVPS); 2024, http://dx.doi.org/10.69766/JNEW6916, 29th edition, providing global analysis of PV market developments in 2023.

[82] Habib S, Tamoor M, Gulzar MM, Chauhdary ST, Ahmad H, Alqahtani M, Khalid M. Design, techno-economic evaluation, and experimental testing of grid connected rooftop solar photovoltaic systems for commercial buildings. Front Energy Res 2024;Volume 12 - 2024. http://dx.doi.org/10.3389/fenrg.2024.1483755.

[83] Kumar S, Nagarajan C. Performance-economic and energy loss analysis of 80 KWp grid connected roof top transformer less photovoltaic power plant. Circuits Syst 2016;7:662–79. http://dx.doi.org/10.4236/cs.2016.76056.

[84] Morrison D, Phillips M. Emerging trends in real estate global outlook 2023. PwC and the Urban Land Institute; 2023, https://www.pwc.com/gx/en/industries/financial-services/assets/uli-emerging-trends-global-report.pdf. [Accessed: April 2024].

[85] Average size of dwelling. Enerdata; 2008, https://entranze.enerdata.net/average-size-of-dwelling.html. [Accessed: April 2024].

[86] Lödl M, Kerber G, Witzmann R, Hoffmann C, Metzger M. Abschätzung des photovoltaik-potentials auf dachflächen in deutschland. In: 11. Symposium energieinnovation. TU München, Fachgebiet Elektrische Energieversorgungsnetze; Siemens AG, Corporate Technology; 2010, https://mediatum.ub.tum.de/doc//%20969497/969497.pdf. [Accessed: April 2024].

[87] Sun L, Chang Y, Wu Y, Sun Y, Su D. Potential estimation of rooftop photovoltaic with the spatialization of energy self-sufficiency in urban areas. Energy Rep 2022;8:3982–94. http://dx.doi.org/10.1016/j.egyr.2022.03.035.

[88] Koch H, Lechner S, Erdmann S, Hofmann M. Assessing the potential of rooftop photovoltaics by processing high-resolution irradiation data, as applied to giessen, Germany. Energies 2022;15(19). http://dx.doi.org/10.3390/en15196991.

[89] Gagnon P, Margolis R, Melius J, Phillips C, Elmore R. Rooftop solar photovoltaic technical potential in the United States: A detailed assessment. National Renewable Energy Laboratory; 2016, https://www.nrel.gov/docs/fy16osti/65298.pdf. [Accessed: April 2024].

[90] Bódis K, Kougias I, Jäger-Waldau A, Taylor N, Szabó S. A high-resolution geospatial assessment of the rooftop solar photovoltaic potential in the European union. Renew Sustain Energy Rev 2019;114:109309. http://dx.doi.org/10.1016/j.rser.2019.109309.

[91] Yang Y, Campana PE, Stridh B, Yan J. Potential analysis of roof-mounted solar photovoltaics in Sweden. Appl Energy 2020;279:115786. http://dx.doi.org/10.1016/j.apenergy.2020.115786.

[92] Kozlovas P, Gudzius S, Ciurlionis J, Jonaitis A, Konstantinaviciute I, Bobinaite V. Assessment of technical and economic potential of urban rooftop solar photovoltaic systems in Lithuania. Energies 2023;16(14). http://dx.doi.org/10.3390/en16145410.

[93] Gutschner M, Ruoss SND, Toggweiler P, Schoen T. Potential for Building Integrated Photovoltaics. International Energy Agency; 2002, https://iea-pvps.org/wp-content/uploads/2020/01/rep7_04.pdf. [Accessed: April 2024].

[94] Mainzer K, Fath K, McKenna R, Stengel J, Fichtner W, Schultmann F. A high-resolution determination of the technical potential for residential-roof-mounted photovoltaic systems in Germany. Sol Energy 2014;105:715–31. http://dx.doi.org/10.1016/j.solener.2014.04.015.

[95] Byrne J, Taminiau J, Kurdgelashvili L, Kim KN. A review of the solar city concept and methods to assess rooftop solar electric potential, with an illustrative application to the city of seoul. Renew Sustain Energy Rev 2015;41:830–44. http://dx.doi.org/10.1016/j.rser.2014.08.023.

[96] Melius J, Margolis R, Ong S. Estimating rooftop suitability for PV: A review of methods, patents, and validation techniques. National Renewable Energy Laboratory; 2013, https://www.nrel.gov/docs/fy14osti/60593.pdf. [Accessed: April 2024].

[97] Pezzutto S, Zambotti S, Croce S, Zambelli P, Garegnani G, Scaramuzzino C, Pascuas RP, Haas F, Exner D, Lucchi E, Valle ND, Zubaryeva A, Müller A, Hartner M, Fleiter T, Klingler A-L, Kühnbach M, Manz P, Marwitz S, Rehfeldt M, Steinbach J, Popovski E. D2.3 WP2 report – open data set for the EU28. 2019, Hotmaps – Heating and Cooling Open Source Tool for Mapping and Planning of Energy Systems, https://www.hotmaps-project.eu/wp-content/uploads/2018/03/D2.3-Hotmaps_for-upload_revised-final.pdf. [Accessed: April 2024].

[98] Electricity consumption per dwelling for electrical appliances and lighting, odyssee-mure. 2023, https://www.odyssee-mure.eu/publications/efficiency-by-sector/households/electricity-consumption-dwelling-electrical-appliances-lighting.html. [Accessed: April 2024].

[99] Photovoltaic geographical information system (PVGIS). European Commission's Joint Research Centre; 2022, https://re.jrc.ec.europa.eu/pvg_tools/en/tools.html. [Accessed: April 2024].

[100] Solar systems 2023. 2023, State of Berlin, https://www.berlin.de/umweltatlas/en/energy/solar-systems/continually-updated/introduction/. [Accessed: April 2024].

[101] BDO AG Wirtschaftsprüfungsgesellschaft, https://www.bdo.de/en-gb/insights/updates/tax-legal/tax-treatment-of-photovoltaic-systems. [Accessed: April 2024].

[102] Electricity prices for household consumers - bi-annual data. Eurostat; 2023, https://ec.europa.eu/eurostat/databrowser/view/NRG_PC_204/default/table?lang=en. [Accessed: April 2024].
[103] Einspeisevergütung 2023: Entwicklung, Tabellen und alle Infos. Zolar; 2023, https://www.zolar.de/blog/eeg-einspeiseverguetung. [Accessed: April 2024].
[104] Gas prices for household consumers - bi-annual data. Eurostat; 2023, https://ec.europa.eu/eurostat/databrowser/view/NRG_PC_202/default/table?lang=en. [Accessed: April 2024].
[105] Gas prices for household consumers - bi-annual data. Eurostat; 2023, https://ec.europa.eu/eurostat/databrowser/view/TEC00118/default/table?lang=en. [Accessed: April 2024].
[106] Reference and discount rates (in %) since 01.08.1997. European Commission; 2023, https://competition-policy.ec.europa.eu/state-aid/legislation/reference-discount-rates-and-recovery-interest-rates/reference-and-discount-rates_en. [Accessed: April 2024].
[107] Real time electricity production emissions by country. Nowtricity; 2023, https://www.nowtricity.com/. [Accessed: April 2024].
[108] Bundesamt für Wirtschaft und Ausfuhrkontrolle (BAFA), https://www.bafa.de/SharedDocs/Downloads/DE/Energie/eew_infoblatt_co2_faktoren_2025.pdf. [Accessed: July 2025].
[109] NUTS classification:The hierarchical categorisation of EU territories and regions. Statistisches Bundesamt (Destatis); 2024, https://www.destatis.de/Europa/EN/Methods/Classifications/OverviewClassification_NUTS.html. [Accessed: April 2024].
[110] Data commons. 2024, https://datacommons.org/place/nuts/DE3. [Accessed: April 2024].
[111] Lämmle M, Herrando M, Ryan G. Basic concepts of PVT collector technologies, applications and markets. SHC Task 60/report D5. International Energy Agency; 2020, https://www.iea-shc.org/Data/Sites/1/publications/IEA-SHC-Task60-D5-Basic-Concepts-of-PVT-Technologies.pdf. [Accessed: April 2024].
[112] Chekir N, Mejbri K, Bellagi A. Simulation d'une machine frigorifique à absorption fonctionnant avec des mélanges d'alcanes. Int J Refrig 2006;29(3):469–75. http://dx.doi.org/10.1016/j.ijrefrig.2005.09.016, Issue with Special Emphasis on Cryobiology.
[113] Djezzar S, Meniai A-H. Modeling of the use of hydrocarbons in absorption refrigeration machine. Chem Eng Trans 2018;69:397–402. http://dx.doi.org/10.3303/CET1869067.
[114] Bellos V, Nalbantis I, Tsakiris G. Friction modeling of flood flow simulations. J Hydraul Eng 2018;144(12):04018073. http://dx.doi.org/10.1061/(ASCE)HY.1943-7900.0001540.
[115] Kovacs P, Persson M, Wahlgren P, Jensen S. Quality assurance in solar thermal heating and cooling technology: pressure drop over a solar flat plate collector using various heat transfer fluids. European Commission; 2012, http://www.estif.org/solarkeymarknew/images/downloads/QAiST/qaist%20d2.2_r2.13%20pressure%20drop.pdf. [Accessed: April 2024].
[116] Herrando M, Markides CN, Hellgardt K. A UK-based assessment of hybrid PV and solar-thermal systems for domestic heating and power: System performance. Appl Energy 2014;122:288–309. http://dx.doi.org/10.1016/j.apenergy.2014.01.061.
[117] Schmidt EF. Wärmeübergang und druckverlust in rohrschlangen. Chem Ing Tech 1967;39(13):781–9. http://dx.doi.org/10.1002/cite.330391302.
[118] Rogers G, Mayhew Y. Heat transfer and pressure loss in helically coiled tubes with turbulent flow. Int J Heat Mass Transfer 1964;7(11):1207–16. http://dx.doi.org/10.1016/0017-9310(64)90062-6.
[119] Fernández-Seara J, Diz R, Fracisco J, Sieres J, Dopazo A. Thermal analysis of a helically coiled tube in a domestic hot water storage tank. 2007, http://hdl.handle.net/2263/45760.
[120] Saad Y. Iterative methods for sparse linear systems. 2nd ed.. SIAM; 2003.
[121] Golub GH, Van Loan CF. Matrix computations. 4th ed.. Johns Hopkins University Press; 2013.